Divergence of Many-Body Perturbation Theory for Noncovalent Interactions of Large Molecules

Brian D. Nguyen, Guo P. Chen, Matthew M. Agee, Asbjörn M. Burow, Matthew P. Tang, and Filipp Furche*

Department of Chemistry, University of California, Irvine, 1102 Natural Sciences II, Irvine, CA 92697-2025, USA

E-mail: filipp.furche@uci.edu

Abstract

Prompted by recent reports of large errors in noncovalent interaction (NI) energies obtained from many-body perturbation theory (MBPT), we compare the performance of second-order Møller–Plesset MBPT (MP2), spin-scaled MP2, dispersion-corrected semilocal density functional approximations (DFA), and the post-Kohn–Sham random phase approximation (RPA) for predicting binding energies of supramolecular complexes contained in the S66, L7, and S30L benchmarks. All binding energies are extrapolated to the basis set limit, corrected for basis set superposition errors, and compared to reference results of the domain-based local pair-natural orbital coupled-cluster (DLPNO-CCSD(T)) or better quality. Our results confirm that MP2 severely overestimates binding energies of large complexes, producing relative errors of over 100% for several benchmark compounds. RPA relative errors consistently range between 5-10%, significantly less than reported previously using smaller basis sets, whereas spin-scaled MP2 methods show limitations similar to MP2, albeit less pronounced, and empirically dispersion-corrected DFAs perform almost as well as RPA. Regression analysis reveals

a systematic increase of relative MP2 binding energy errors with the system size at a rate of approximately 0.1% per valence electron, whereas the RPA and dispersion-corrected DFA relative errors are virtually independent of the system size. These observations are corroborated by a comparison of computed rotational constants of organic molecules to gas-phase spectroscopy data contained in the ROT34 benchmark. To analyze these results, an asymptotic adiabatic connection symmetry-adapted perturbation theory (AC-SAPT) is developed which uses monomers at full coupling whose ground-state density is constrained to the ground-state density of the complex. Using the fluctuation–dissipation theorem, we obtain a nonperturbative "screened second-order" expression for the dispersion energy in terms of monomer quantities which is exact for non-overlapping subsystems and free of induction terms; a first-order RPA-like approximation to the Hartree, exchange, and correlation kernel recovers the macroscopic Lifshitz limit. The AC-SAPT expansion of the interaction energy is obtained from Taylor expansion of the coupling strength integrand. Explicit expressions for the convergence radius of the AC-SAPT series are derived within RPA and MBPT and numerically evaluated. Whereas the AC-SAPT expansion is always convergent for nondegenerate monomers when RPA is used, it is found to spuriously diverge for second-order MBPT, except for the smallest and least polarizable monomers. The divergence of the AC-SAPT series within MBPT is numerically confirmed within RPA; prior numerical results on the convergence of the SAPT expansion for MBPT methods are revisited and support this conclusion once sufficiently high orders are included. The cause of the failure of MBPT methods for NIs of large systems is missing or incomplete "electrodynamic" screening of the Coulomb interaction due to induced particle–hole pairs between electrons in different monomers, leaving the effective interaction too strong for AC-SAPT to converge. Hence, MBPT cannot be considered reliable for quantitative predictions of NIs, even in moderately polarizable molecules with a few tens of atoms. The failure to accurately account for electrodynamic polarization makes MBPT qualitatively unsuitable for applications such as NIs of nanostructures, macromolecules, and soft materials; more robust non-perturbative approaches such as RPA or coupled

cluster methods should be used instead whenever possible.

1 Introduction

While covalent bonding is a central paradigm of chemical theory, noncovalent interactions (NIs)[1,2] are often considered secondary due to their "weakness." For small molecules with 10 or less atoms, NIs are at least one order of magnitude smaller than covalent bonds, and their low chemical specificity makes them difficult to detect and control. However, it has long been recognized that NIs are pairwise nonadditive and can grow superlinearly with system size.[3–5] Indeed, NIs are key factors determining conformation, tertiary structure, and other properties of molecular aggregates and complexes,[6–8] materials,[9,10] or molecular crystals.[11,12] Recent advances in experimental techniques such as molecular beam spectroscopy[13] have made NIs readily observable in larger molecular systems, and even areas focused on covalent bonding such as synthetic chemistry and catalysis increasingly use NIs to fine-tune reactivity and selectivity.[14,15]

Perhaps with the exception of density functional theory, most electronic structure methods have been developed and tested for small molecules. A central assumption underlying this "bottom-up" approach is that methods performing well for small systems may be scaled up to larger ones without deterioration in accuracy. Size consistency and size extensivity[16–18] are often assumed to be sufficient to ensure that the accuracy of an electronic structure method for chemical processes is approximately independent of the system size. Møller–Plesset (MP) many-body perturbation theory (MBPT),[19] which is based on the Fock operator as a zeroth-order Hamiltonian, has enjoyed much popularity as one of the least expensive yet useful ab-initio correlated electronic methods; size-extensivity of the energy is an often cited advantage of MP theory.[16] Moreover, unlike semilocal density functional approximations (DFAs), whose performance for NIs can be erratic,[20–22] MBPT has widely been considered a qualitatively suitable starting point for modeling NIs, particularly in systems too large to be tractable by

more advanced methods.[23–25] This view appears to have emerged from the correct $1/R^6$ behavior of the dispersion energy obtained from MBPT as well as early favorable convergence for small closed-shell systems.[26,27] In a landmark 1993 paper,[26] Moszynski, Jeziorski, and Szalewicz investigated the convergence of the MBPT expansion of the dispersion energy for several small weakly bound complexes and concluded that convergence of the series is "very fast." This may be contrasted with covalent interactions, where MBPT is known to diverge in many systems of chemical interest.[28–30] The assumption that "weak" closed-shell interactions between distant electron pairs are accurately captured by MBPT is implicit in many applications as well as theoretical approaches such as local correlation methods.[31] Against the backdrop of the qualitative inability of semilocal DFAs to capture long-range NIs, this assumption has also motivated the development of efficient computational methods to apply MBPT to systems with 100 and more atoms.[32–36]

However, with the expanding scope of MBPT applications during the past two decades, an increasing number of examples were reported that shows substantial overestimation of NI energies by second-order MP MBPT (MP2).[37] In 2010, Pulay and co-workers pointed out that MP2 overbinds coronene dimer by almost 100% compared to the quadratic configuration interaction reference data.[38,39] Comparing initially to solution phase thermodynamic data[40] and later to coupled cluster singles, doubles, and perturbative triples (CCSD(T)) calculations,[41] Grimme noted that the accuracy of MP2 severely deteriorates for supramolecular systems.[42] Initially, these deviations were viewed as the result of a quantitative rather than qualitative shortcomings of MBPT, which led to the development of empirical correction schemes such as spin-component-scaled MP2 methods[43,44] and MP2.5.[24] For large molecular complexes, the shortcomings of pairwise additive methods such as MP2 have been ascribed to missing three- and higher-body dispersion interactions,[42] triggering the development of dispersion corrections including MP2C,[45–47] MP2D,[48,49] as well as empirical three-,[42,50] and many-body[51] dispersion corrections for DFAs. Meanwhile, Dobson and co-workers showed that the simple addition of pairwise $1/R^6$ interactions yields qualitatively incorrect asymp-

totic power laws for dispersion interactions between macroscopic solids. For example, the interaction between two large parallel graphene sheets decays as $1/D^3$ with the distance D between the sheets, whereas finite-order MBPT yields a $1/D^4$ behavior.[52,53] These troubling inconsistencies and the sheer magnitude of the errors raise the question whether and to what extent MBPT is fundamentally adequate for NIs of large but finite molecules.

To address this question, we revisit the performance of MBPT with particular emphasis on large molecules with 100 and more atoms, and contrast it with the random phase approximation (RPA) to the ground-state correlation energy in a density functional context.[54–56] Particle–hole RPA may be viewed as a resummation of ring diagrams[57] which correspond to direct Coulomb interactions between particle–hole pairs and constitute the most long-ranged correlation contribution to the interaction energy between closed-shell systems.[2,58] Indeed, the accuracy of RPA for NIs in small molecules,[59,60] rare-gas solids,[61] and layered materials[53] is well documented, but few results for intra- and intermolecular NIs in large systems are available.[62,63] Building on efficient RPA implementations for energy[64] and analytic derivatives,[65] we investigate the size-dependence of MBPT and RPA interaction energies using the S66,[66,67] L7,[68] and S30L[69] benchmarks in Section 3. These benchmarks contain systems ranging from 6 to 204 atoms, with binding energies between 1 kcal/mol and 136 kcal/mol. To evaluate whether our observations for energetics also hold for structures, we also compare rotational constants from MP2, RPA, and Grimme's dispersion corrected DFA-D3[42] structure optimizations to gas-phase spectroscopy data using organic molecules with 18–35 atoms from the ROT34 benchmark set.[70,71]

In Section 4, these results are analyzed in detail using a symmetry-adapted perturbation theory (SAPT) type[72,73] asymptotic theory of NIs between closed-shell fragments whose ground-state density is constrained to the supersystem ground-state density using a local one-body potential in the spirit of the adiabatic connection (AC)[54,55,74,75] in density functional theory (DFT). This leads to a compact, non-perturbative expression for the dispersion energy, as well as explicit estimates for the convergence radius of the AC-SAPT expansion.

We investigate how the estimated convergence radii correlate with errors of MP2 and RPA calculations of NIs and the system size. A numerical model for the divergence of the AC-SAPT expansion for moderately large and polarizable systems is obtained by re-expansion of the RPA correlation energy into powers of the interaction. Conclusions for electronic structure theory and computational practice are presented in Sec. 5.

2 Methods

2.1 Computational Details

MP2 energies were evaluated using on self-consistent Hartree–Fock (HF) orbitals. Variants of MP2 such as spin-component-scaled MP2 (SCS-MP2)[43] and scaled opposite-spin MP2 (SOS-MP2)[44] were also assessed. All MP2 calculations were performed with the RI approximation (RI-MP2) using the `ricc2` module[76] of TURBOMOLE.[77]

RPA energies and analytic derivatives were obtained in a post-Kohn–Sham (KS) fashion, i.e., a KS calculation using a semilocal DFA was first performed to obtain the KS orbitals, and subsequently the exact exchange energy and the RPA correlation energy were evaluated non-self-consistently. The Perdew–Burke–Ernzerhof (PBE)[78] and Tao–Perdew–Staroverov–Scuseria (TPSS)[79] DFAs were used for the KS calculations; the ensuing RPA calculations, dubbed RPA(PBE) and RPA(TPSS), respectively, employed the resolution-of-the-identity (RI) approximation and the imaginary frequency integration technique as implemented in the `rirpa` module[64] of TURBOMOLE.[77] Perturbative order-by-order analysis of the RPA correlation energies was carried out using a modified version of TURBOMOLE 7.3.

Tight convergence criteria of 10^{-9} Hartrees for the energy and 10^{-7} atomic units (a.u.) for the root mean square change of the one-particle density matrix were used for the KS and HF self-consistent field iterations. DFA quadrature grids of m5 quality[80] were used for the KS reference calculations. Imaginary frequency grids of 100 points were employed for the RPA energy calculations. Interaction energies were computed based on the supermolecular

approach and extrapolated to the complete basis set (CBS) limit, as detailed in the next subsection. RPA structural optimizations[65] of molecules in the ROT34 benchmark set were converged to a maximum Cartesian gradient norm $\leq 10^{-4}$ a.u. and 10^{-7} a.u. in the energy change. Fine imaginary frequency grids of 200 points were used for RPA gradient calculations and structure optimizations.

The interaction energies were benchmarked against CCSD(T) values for the S66 benchmark set[66,67] and against the domain-based local pair-natural orbital (DLPNO) based CCSD(T) calculations for the L7 and S30L benchmark sets.[81,82] DLPNO-CCSD(T) results can vary significantly for weakly bound complexes depending on the truncation of the PNO basis and domain size.[83,84] Moreover, even with tight truncation thresholds, the results may differ by up to ∼2 kcal/mol based on the choice of basis set and basis-set extrapolation scheme as seen by Refs. 82 and 84. For the present study, the DLPNO-CCSD(T) reference values were taken from Brandenburg *et al*[82] employing the "TightPNO" truncation thresholds[83] and the basis-set extrapolation scheme from Ref. 85 for both the L7 and S30L benchmarks. Throughout the paper, signed errors are defined as differences between calculated and reference values; for example, a positive error in binding energies signifies underbinding.

2.2 Basis Set Convergence

The RPA total energy is the sum of the energy expectation value of the KS determinant, i.e., the sum of the zeroth- and first-order energies, and the RPA correlation energy. These two parts of the energy exhibit qualitatively different basis set convergence.[86] The energy expectation value of the KS determinant was evaluated within the RI-JK algorithm with the corresponding optimized auxiliary basis sets.[87] Karlsruhe segmented-contracted polarized quadruple-ζ (def2-QZVP) basis sets[88,89] were chosen for the KS reference calculations because they were found to yield significantly faster convergence of the KS energy expectation value than the corresponding correlation-consistent basis sets using generalized contractions.[90–92]

RPA correlation energies were evaluated using Dunning's correlation-consistent polarized valence basis sets[90,91] in conjunction with the corresponding auxiliary correlation-consistent basis sets optimized for RI-MP2.[92,93] Small core relativistic effective core potentials[94,95] were used for the halogen atoms in the S30L[69] benchmark set. The frozen core approximation was employed for the RPA correlation energy calculations. Basis set superposition error was estimated by 50% counterpoise (CP) correction as recommended by Risthaus and coworkers;[96] the CP correction was only applied to the RPA correlation energy.

The CBS limit of the RPA correlation energy was estimated using the two-point $1/X^3$ extrapolation, where $X = 3$ (triple-ζ), 4 (quadruple-ζ), etc.[86,97] Dunning's correlation-consistent polarized triple- (cc-pVTZ) and quadruple-ζ (cc-pVQZ) valence basis sets[90,91] were employed for the 3-4 extrapolation. The basis set dependence of the S30L interaction energies is displayed in Figure 1. To assess the residual basis set error, exploratory calculations were performed using Dunning's cc-pV5Z basis sets[92] for the pincer complex with 2,4,7-trinitro-9-fluorenone as the guest molecule (TNF@tweezer2, compound 5).[69] The 4-5 extrapolation was found to be within 0.20 kcal/mol compared to the 3-4 extrapolation, see Figure S1 in the Supporting Information.

Similarly, correlation energies from MP2 and its variants were obtained using the frozen core approximation, 50% CP correction, and the 3-4 extrapolation using cc-pVTZ and cc-pVQZ basis sets.[90,91] HF energies were computed using def2-QZVP basis set.[88,89]

For the ROT34 benchmark,[70,71] def2-QZVP basis sets were used for both the KS expectation value and the RPA correlation; core electrons were treated explicitly. This approach is expected to yield RPA structures of near basis-set limit quality.[65] Indeed, changing the basis sets from def2-TZVP to def2-QZVP only yields a small but systematic decrease in the error in the RPA rotational constants, see Supporting Information.

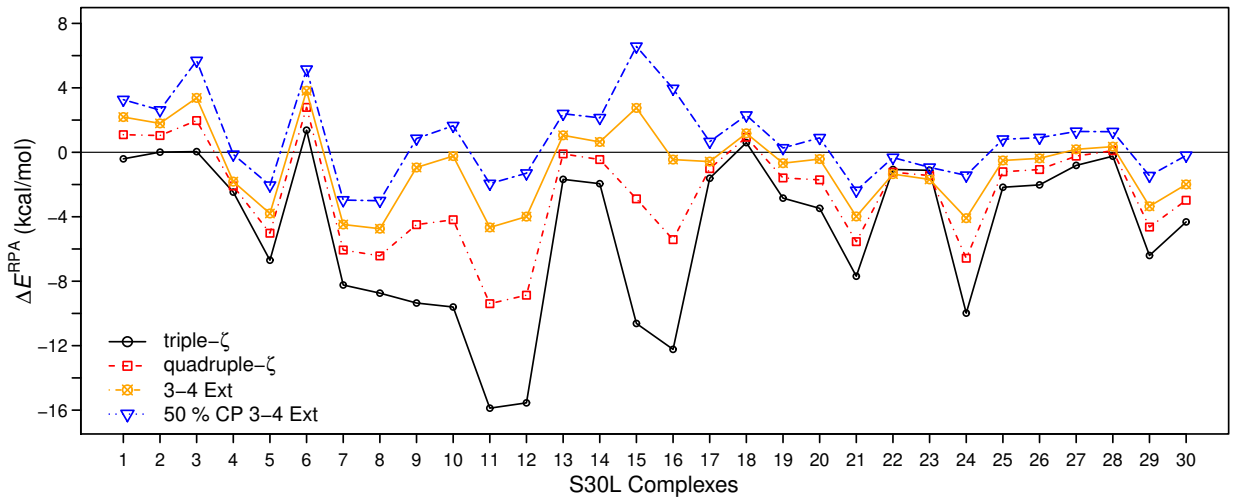

Figure 1: S30L interaction energy errors (ΔE^{RPA}) computed using RPA(PBE) with correlation-consistent triple-ζ and quadruple-ζ basis sets, as well as using triple-quadruple (3-4) extrapolation with 50% and without counterpoise (CP) correction. DLPNO-CCSD(T) reference values are from Caldeweyher *et al.*[81]

3 Results

3.1 S66, L7, and S30L Interaction Energy Benchmarks

The S66 benchmark consists of binding energies of 66 complexes ranging from 6 to 34 atoms; the average binding energy is 5.50 kcal/mol.[66,67] This benchmark set is divided into groups featuring hydrogen bonding, π–π stacking, aliphatic–aliphatic interactions, π–aliphatic interactions, and other nonspecific interactions, respectively. For the binding energies of these complexes, MBPT is accurate: MP2 and third-order MP MBPT (MP3) yield mean absolute errors (MAEs) of 0.35 kcal/mol and 0.47 kcal/mol, respectively. The errors of dispersion-corrected DFT and MP2 variants are comparable. The good performance of dispersion corrected DFAs is hardly surprising here since S66 is part of commonly used training sets for parameter estimation.[50]

The L7 benchmark contains binding energies of seven complexes: Octadecane dimer, guanine trimer, circumcoronene–adenine dimer, coronene dimer, guanine–cytosine dimer, circumcoronene–guanine–cytosine dimer, and an amyloid fragment trimer containing phenylalanine residues; the average binding energy is 16.7 kcal/mol.[68,82] As shown in Table 1, MP2

Table 1: Mean absolute errors (MAE), mean errors (ME), and absolute minimum-maximum error range (MinMax) in kcal/mol of various methods at complete basis set limit for the S66, L7, and S30L test sets. Positive ME corresponds to underbinding.

	S66			L7			S30L		
Methods	MAE	ME	MinMax	MAE	ME	MinMax	MAE	ME	MinMax
RPA(PBE)	0.61	0.61	1.00	1.72	1.47	3.53	2.03	0.82	6.44
RPA(TPSS)	0.63	0.63	1.02	1.92	1.73	3.75	2.05	1.33	8.64
MP2	0.35	−0.54	2.30	8.77	−8.77	17.51	18.74	−18.74	66.07
MP3[a]	0.47	0.47	1.93	6.71	6.26	13.13	−−	−−	−−
SCS-MP2	0.32	0.64	1.92	2.49	−1.41	5.77	7.43	−4.68	33.47
SOS-MP2	0.65	1.23	2.57	2.28	2.27	5.83	6.26	2.35	16.26
PBE-D3[b]	0.34	−0.24	1.93	1.91	0.92	4.39	3.06	1.83	9.80
PBE-D4[b]	0.34	−0.30	1.66	1.71	0.16	2.44	2.94	−0.77	9.30
PW6B95-D3[b]	−−	−−	−−	1.39	1.19	2.20	1.82	0.32	4.70
PW6B95-D4[b]	−−	−−	−−	1.80	1.40	3.30	2.02	0.96	4.10

[a] MP3 values from Refs. 66 and 68.
[b] Dispersion corrected DFA values for L7 and S30L from Ref. 81.

performs poorly with an MAE of 8.10 kcal/mol, which is an order of magnitude more larger for S66. Aside from the dependence of errors on system size discussed in Section 4.6.2, MP2 is known to systematically overestimate π–π stacking interactions even in smaller systems.[66] The inclusion of higher orders does not systematically improve the MBPT results. For both, the S66 and L7 benchmark sets, MP2 and MP3 mean errors are on the same orders of magnitude but of opposite sign. Empirically, one observes that odd MBPT orders tend to produce underbinding, whereas even orders produce overbinding.[29,30] The poor performance of MBPT for L7 and especially S30L is in sharp contrast to the one observed for RPA, dispersion corrected PBE-D3, and the recently developed PBE-D4,[50] which all yield MAEs in the range of 2 kcal/mol. The RPA L7 results reported here are $\sim 50\%$ more accurate than the ones previously obtained using def2-TZVP basis sets,[98] underlining the importance of basis set extrapolation for RPA interaction energy benchmarks.[86]

The S30L benchmark set contains binding energies of 30 large supramolecular complexes including π stacking and CH–π interactions, hydrogen and halogen bonding, and charged species; the average binding energy is 37.5 kcal/mol.[69,82] MP2 exhibits severe overbinding for most species, producing spectacular errors > 60 kcal/mol for the π stacked complexes

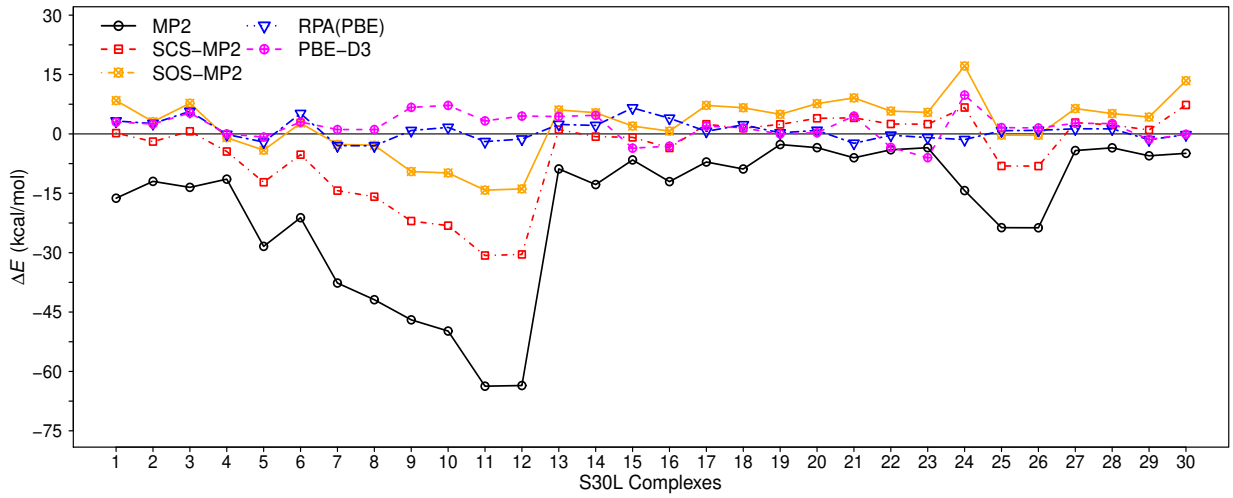

Figure 2: S30L interaction energy errors (ΔE) for MP2 variants, RPA(PBE), and dispersion corrected PBE-D3. MP2 and RPA(PBE) results are 3-4 extrapolated, and PBE-D3 results use def2-QZVP basis sets. DLPNO-CCSD(T) reference values are from Caldeweyher *et al.*[81]

11 and 12, see Figure 2 and Table 1. With MAEs of 7.43 and 6.26 kcal/mol, SCS-MP2 and the SOS-MP2 inherit the shortcomings of MP2 to a significant degree. RPA yields MAEs close to 2 kcal/mol regardless of the KS reference, consistent with its performance observed for L7. Dispersion corrected DFAs show comparable MAEs, but behave less systematically than RPA, as evidenced by somewhat larger absolute minimum-maximum error ranges. The present S30L results for RPA are more than twice as accurate as the ones reported by Heßelmann for the S12L subset;[62] this is likely a consequence of the improved CCSD(T) reference values[81] used here as well as better controlled basis set errors.

3.2 ROT34: Intramolecular Interactions

To investigate whether the strong performance of RPA for intermolecular binding energies translates to other properties such as molecular structures of larger flexible molecules, the equilibrium structures of 34 organic molecules contained in the ROT34 benchmark[70,71] were optimized using RPA with def2-QZVP basis sets; rotational constants were calculated in the rigid rotor approximation. Rotational constants are a sensitive measure of intramolecular mid- and long-range interactions, and accurate experimental values are available from gas-

phase rotational spectroscopy.[70,71]

As displayed in Figure 3, the PBE DFA produces a MAE of 18.2 MHz, even with D3 dispersion correction; the Minnesota DFA M06L[99] and the strongly constrained and appropriately normed (SCAN)[100] DFA perform significantly better:[101] For SCAN, SCAN-D3, and M06L MAEs of 3.7 MHz, 3.3 MHz, and 4.0 MHz were reported.[101] The MAEs of MP2 and SCS-MP2, on the other hand, are 5.5 MHz and 5.4 MHz,[71] respectively, comparing unfavorably with the RPA(PBE) result of 3.1 MHz; using the TPSS instead of the PBE DFA to generate the KS reference yields an almost identical MAE of 3.0 MHz. Thus, even for the moderately sized systems contained in ROT34, the sub-par performance of MP2 is notable.

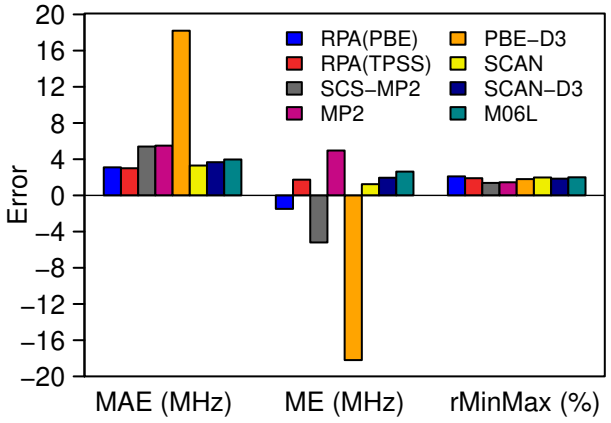

Figure 3: Errors in ROT34 computed rotational constants compared to experiment.[71] Mean absolute errors (MAE) and mean errors (ME) are in MHz, and relative minimum-maximum error ranges (rMinMax) are in %. MP2 and SCS-MP2 results are from Ref. 71; and SCAN, SCAN-D3, PBE-D3, and M06L results are from Ref. 101.

4 AC-SAPT Analysis

4.1 Statement of the Problem

In the following, the results of the previous sections are analyzed in two steps: First, we derive asymptotically exact expressions for the dispersion energy at large separation. We rely on the general SAPT partitioning of the Hamiltonian,[73] but unlike prior DFT-SAPT

methods[102,103] or van-der-Waals inclusive frozen density embedding,[104,105] the present AC-SAPT approach uses density functional theory only for the inter-fragment interaction and constrains the density of the monomers, leading to compact closed-form expressions for the interaction energy and a separation of dispersion and induction effects. We derive an upper bound for the convergence radius of the resulting AC-SAPT expansion. Second, we show that the RPA dispersion energy corresponds to a partial resummation of the AC-SAPT expansion, whereas the MBPT dispersion energy corresponds to a finite-order approximation. When the monomers are treated within RPA, the AC-SAPT converges for nondegenerate monomers, whereas it is found to be susceptible to spurious divergence for MBPT treatments of the monomers.

We consider a molecular supersystem or complex A–B consisting of two non-overlapping subsystems or fragments A and B, i.e., the inter-fragment distance R is assumed to be so large that the overlap between the two ground states is exponentially small. Since there is vanishing charge transfer in this limit, the fragments have integer electron numbers $N_\mathrm{A}, N_\mathrm{B}$ with ground states resembling the lowest-energy separated fragment (dissociation) limit of A–B. The Born–Oppenheimer Hamiltonian of the supersystem at coupling strength α is

$$\hat{H}^\alpha = \hat{H}_\mathrm{A} + \hat{H}_\mathrm{B} + \alpha \hat{V}_{ee\,\mathrm{int}} + \hat{V}^\alpha_{s\,\mathrm{int}}[\rho], \tag{1}$$

where $\hat{H}_\mathrm{A}$ and $\hat{H}_\mathrm{B}$ denote the N_A- and N_B-electron Hamiltonians of the isolated subsystems, and $\hat{V}_{ee\,\mathrm{int}}$ is the operator of the electron-electron Coulomb interaction *between* A and B. The supersystem eigenstates $|\Psi^\alpha_n\rangle$, which are constrained to be antisymmetric under any permutations of electrons in the supersystem as in conventional SAPT, and their energies E^α_n are defined by

$$\hat{H}^\alpha |\Psi^\alpha_n\rangle = E^\alpha_n |\Psi^\alpha_n\rangle . \tag{2}$$

$\hat{V}^\alpha_{s\,\mathrm{int}}[\rho]$ represents a local one-electron potential which constrains the density of the supersystem ground state $|\Psi^\alpha_0\rangle$ to the physical ground-state density $\rho = \rho^1 = \rho^\alpha|_{\alpha=1}$. Since $\hat{V}^\alpha_{s\,\mathrm{int}}[\rho]$

is a unique functional of ρ,[106] so are $|\Psi_n^\alpha\rangle$ and the corresponding energies E_n^α. Throughout this paper, the ground state $|\Psi_0^\alpha\rangle$ is assumed to be nondegenerate for finite R, a mild condition typically satisfied for interacting closed-shell fragments. The use of symmetry adaption implies that the present approach is valid only at large R as in conventional SAPT,[107] but this is sufficient for asymptotic analysis.

In analogy with the conventional KS potential,

$$\hat{V}_{s\,\mathrm{int}}^{\alpha}[\rho] = \hat{V}_{ne\,\mathrm{int}} + V_{nn\,\mathrm{int}} + \hat{V}_{\mathrm{int}}^{\mathrm{HXC}}[\rho] - \hat{V}_{\mathrm{int}}^{\alpha\mathrm{HXC}}[\rho] \tag{3}$$

may be defined as a sum of the "external" one-electron nucleus-electron potential $\hat{V}_{ne\,\mathrm{int}}$ and the constant nucleus-nucleus attraction $V_{nn\,\mathrm{int}}$ between the fragments plus a remainder accounting for Hartree-, exchange-, and correlation (HXC) effects. At full coupling ($\alpha = 1$), the HXC part of $\hat{V}_{s\,\mathrm{int}}^{\alpha}[\rho]$ vanishes, whereas at $\alpha = 0$, $\hat{V}_{s\,\mathrm{int}}^{\alpha}[\rho]$ equals the KS potential arising from the interaction between the fragments. Since the KS potential is spatially local, it additively separates into A and B parts for large R, giving rise to a unique partitioning of the supersystem density into a sum of subsystem densities, i.e., $\rho(x) = \rho_{\mathrm{A}}(x) + \rho_{\mathrm{B}}(x)$. Thus, the present approach is closely related to partition DFT (PDFT).[108,109] However, PDFTs[102,103] and related embedding schemes[104,105] typically start from a KS-DFT calculation of the supersystem, whereas here the fragment ground states corresponding to $\alpha = 0$ include the full intra-fragment electron-electron interaction and therefore are generally not Slater determinants.

4.2 Interaction Energy

We define the A–B interaction energy as the difference in the ground state energies at full and zero coupling,

$$E_{\mathrm{int}}[\rho] = E_0^1[\rho] - E_0^0[\rho]. \tag{4}$$

Using the Hellman–Feynman theorem, the interaction energy may be expressed as a coupling strength average of the potential energy of interaction,[109]

$$E_{\mathrm{int}}[\rho] = \int_0^1 d\alpha\, W^\alpha[\rho], \tag{5}$$

where $W^\alpha[\rho] = dE_0^\alpha/d\alpha = \langle\Psi_0^\alpha|\hat{V}_{ee\,\mathrm{int}}|\Psi_0^\alpha\rangle$; one-electron contributions vanish upon coupling strength integration due to the density constraint. The AC-SAPT expansion of the interaction energy is obtained by expansion of the interacting ground state and the corresponding energy into powers of α, analogous to Görling–Levy perturbation theory.[110,111] Equivalently, the coupling strength integrand W^α may be expanded around $\alpha = 0$, yielding the AC-SAPT series expansion of the interaction energy,

$$E_{\mathrm{int}}[\rho] = \int_0^1 d\alpha \sum_{k=0}^{\infty} \alpha^k W^{(k)}[\rho] = \sum_{k=0}^{\infty} \frac{1}{k+1} W^{(k)}[\rho]. \tag{6}$$

The first-order interaction energy results from evaluating the integrand at $\alpha = 0$,

$$E_{\mathrm{int}}^{(1)}[\rho] = \langle\Psi_0^0|\hat{V}_{ee\,\mathrm{int}}|\Psi_0^0\rangle = E_{\mathrm{int}}^{\mathrm{HX}}[\rho] = \int dx_1 dx_2 \frac{\rho_A(x_1)\rho_B(x_2) - \gamma_A(x_1,x_2)\gamma_B(x_2,x_1)}{|\mathbf{r}_1 - \mathbf{r}_2|}, \tag{7}$$

where $|\Psi_0^0\rangle$ is the antisymmetrized product of the two fragment density-constrained ground-state wavefunctions with one-particle density matrices γ_A, γ_B. As in standard SAPT, the first-order interaction energy is electrostatic and corresponds to the sum of the Hartree and exchange (HX) interactions between the two fragments; unlike in standard SAPT, and as discussed in detail below, the interaction arises from the electrons only. The exchange term is exponentially small for non-degenerate ground states in the large R limit.

The remaining correlation part of the interaction energy,

$$E_{\mathrm{int}}^{\mathrm{C}}[\rho] = \int_0^1 d\alpha \left(\langle\Psi_0^\alpha|\hat{V}_{ee\,\mathrm{int}}|\Psi_0^\alpha\rangle - \langle\Psi_0^0|\hat{V}_{ee\,\mathrm{int}}|\Psi_0^0\rangle\right) \tag{8}$$

is due to dispersion and does not contain any terms describing changes in the fragment densities as the interaction is turned on. The purely dispersive character of the interaction becomes apparent from a factorization of $\hat{V}_{ee\,\mathrm{int}}$ in a fashion analogous to Eqs. (6)-(13) of Ref. 112 and neglecting exponentially small exchange terms, yielding

$$E_{\mathrm{int}}^{\mathrm{C}}[\rho] = \int_0^1 d\alpha \int dx_1 dx_2 \frac{\langle \Psi_0^\alpha | \Delta\hat{\rho}_A(x_1) \Delta\hat{\rho}_B(x_2) | \Psi_0^\alpha \rangle - \langle \Psi_0^0 | \Delta\hat{\rho}_A(x_1) \Delta\hat{\rho}_B(x_2) | \Psi_0^0 \rangle}{|\mathbf{r}_1 - \mathbf{r}_2|}, \qquad (9)$$

where $\Delta\hat{\rho}_A(x) = \hat{\rho}_A(x) - \rho_A(x)$ is the density fluctuation operator associated with fragment A, $\hat{\rho}_A(x)$ is the corresponding density operator, and $\Delta\hat{\rho}_B(x)$ is defined analogously. As opposed to standard SAPT (including DFT-SAPT), which is based on a partitioning of the Hamiltonian that includes induction effects to all orders, the interaction energy in the present approach does not contain any induction terms and is exclusively due to electrostatic (Hartree plus exchange) and dispersion. Factorization of the density operator product in Eq. (9) using the completeness of the eigenstates of $\hat{H}^\alpha$ yields a spectral sum over Hartree interactions between the A and B parts of ground-to-n-th excited state transition densities $\rho_{0n}^\alpha(x) = \rho_{n0}^{\alpha *}(x)$,

$$E_{\mathrm{int}}^{\mathrm{C}}[\rho] = \sum_{n \neq 0} \int_0^1 d\alpha \int dx_1 dx_2 \frac{\rho_{0n\,A}^\alpha(x_1) \rho_{n0\,B}^\alpha(x_2) - \rho_{0n\,A}^0(x_1) \rho_{n0\,B}^0(x_2)}{|\mathbf{r}_1 - \mathbf{r}_2|}. \qquad (10)$$

The $\alpha = 0$ term vanishes for large R since excitations of the non-interacting monomers are localized on either monomer, but is included here to emphasize the analogy to general RPA theory.[113] In this sense, the A–B dispersion energy is given exactly by the Hartree interaction between "electrodynamic" density fluctuations of the monomers. While similar ideas are implicit, e.g., in molecular quantum electrodynamics,[114] the present approach yields a compact, exact expression valid beyond perturbation theory. The induction energy, on the other hand, appears as the difference between the non-interacting ($\alpha = 0$) monomer ground

state energies with and without density constraint,

$$E_{\mathrm{ind}} = E^0[\rho] - E_{\mathrm{A}} - E_{\mathrm{B}}. \tag{11}$$

The total dissociation energy of the complex A–B is thus

$$D_{\mathrm{A\text{–}B}} = E_{\mathrm{int}}[\rho] + E_{\mathrm{ind}}. \tag{12}$$

Induction effects are comparatively small for large R;[115] hence, we will focus on $E_{\mathrm{int}}[\rho]$ in the following.

If the zero-point fluctuation–dissipation theorem (FDT) is invoked[2,54,55,74,75] to factorize the products of fluctuation operators in Eq. (9), the dispersion energy may be expressed as

$$E_{\mathrm{int}}^{\mathrm{C}}[\rho] = -\frac{1}{2}\int_0^1 d\alpha \int_{-\infty}^{\infty} \frac{dz}{2\pi i} \left\langle \left(\mathbf{\Pi}^{\alpha}(z) - \mathbf{\Pi}^{0}(z)\right) \mathbf{V}_{\mathrm{int}} \right\rangle. \tag{13}$$

Here, $\mathbf{\Pi}^{\alpha}(z)$ is the time-ordered supersystem polarization propagator at coupling strength α and imaginary frequency $z = i\omega \in i\mathbf{R}$ defined as[116]

$$\mathbf{\Pi}^{\alpha}(z) = -\sum_{n\neq 0} \left\{ \frac{\boldsymbol{\gamma}_{0n}^{\alpha} \otimes \boldsymbol{\gamma}_{0n}^{\alpha\dagger}}{z - \Omega_n^{\alpha} + i0^+} - \frac{\boldsymbol{\gamma}_{0n}^{\alpha\dagger} \otimes \boldsymbol{\gamma}_{0n}^{\alpha}}{z + \Omega_n^{\alpha} - i0^+} \right\}. \tag{14}$$

$\Omega_n^{\alpha} = E_n^{\alpha} - E_0^{\alpha}$ is the energy of an excitation from $|\Psi_0^{\alpha}\rangle$ to $|\Psi_n^{\alpha}\rangle$, and $\boldsymbol{\gamma}_{0n}^{\alpha}$ denotes the corresponding one-particle transition density matrix. Eq. (14) shows that, for non-degenerate monomer ground states, $\mathbf{\Pi}^{\alpha}(z)$ is a self-adjoint and negative semidefinite operator on the tensor-product space of one-particle operators. $\mathbf{V}_{\mathrm{int}}$ represents the bare inter-fragment electron-electron Coulomb interaction or the Hartree kernel on the same space.

Eqs. (9)-(10) could also be used to define the dispersion energy in conjunction with MP-style partitioning of the Hamiltonian, using the analogous, albeit approximate, HF-based AC framework.[112] Formally, this corresponds to replacing the local exchange-correlation

potential in Eq. (3) with the non-local HF exchange potential. The $\alpha = 0$ reference of this approach is equivalent to monomers with full intra-fragment electron-electron interaction whose inter-fragment interaction is treated at the Hartree plus exchange level. In the HF-based AC framework, the interaction energy obtained from coupling strength integration contains additional induction effects resulting from changes in the fragment densities due to inter-fragment correlation which are not captured by the FDT, but the present conclusions for the dispersive part of the interaction energy remain valid.

4.3 Dispersion Energy

Expression (13) for the dispersion energy can be further re-cast by noting that any contributions from charge transfer excitations between the fragments vanish exponentially due to exponentially vanishing overlap at large R; it therefore suffices to consider $\mathbf{\Pi}^\alpha(z)$ on the domain of fragment-centered excitations only. Thus, $\mathbf{\Pi}^\alpha(z)$ may be partitioned as

$$\mathbf{\Pi}^\alpha(z) = \begin{pmatrix} \mathbf{\Pi}^\alpha_{\mathrm{AA}}(z) & \mathbf{\Pi}^\alpha_{\mathrm{AB}}(z) \\ \mathbf{\Pi}^\alpha_{\mathrm{BA}}(z) & \mathbf{\Pi}^\alpha_{\mathrm{BB}}(z) \end{pmatrix}, \tag{15}$$

where indices AA refer to the 4-index tensor space spanned by products of transition density matrices centered on fragment A, etc. In the non-interacting ($\alpha = 0$) case, all excitations are either excitations of A or B only, hence $\mathbf{\Pi}^0_{\mathrm{AB}}(z) = \mathbf{\Pi}^0_{\mathrm{BA}}(z) = \mathbf{0}$, and the diagonal parts reduce to the fragment polarization propagators (at full intra-fragment coupling). The inter-fragment Coulomb interaction may be partitioned as

$$\mathbf{V}_{\mathrm{int}} = \begin{pmatrix} \mathbf{0} & \mathbf{V}_{\mathrm{AB}} \\ \mathbf{V}_{\mathrm{BA}} & \mathbf{0} \end{pmatrix}, \tag{16}$$

where the diagonal blocks must vanish to recover the correct monomer limit at large R.

It is instructive to introduce the dielectric operator $\boldsymbol{\epsilon}^\alpha(z)$ (also called generalized dielectric

function or matrix[117,118]) via

$$\boldsymbol{\Pi}^{\alpha}(z) = \boldsymbol{\epsilon}^{\alpha}(z)^{-1}\boldsymbol{\Pi}^{0}(z). \tag{17}$$

In the spirit of the Bethe–Salpeter equation,[116] $\boldsymbol{\epsilon}^{\alpha}(z)$ may be expressed as

$$\boldsymbol{\epsilon}^{\alpha}(z) = \mathbf{1} - \boldsymbol{\Pi}^{0}(z)\mathbf{K}_{\mathrm{int}}^{\alpha\mathrm{HXC}}(z), \tag{18}$$

where $\mathbf{K}_{\mathrm{int}}^{\alpha\mathrm{HXC}}(z)$ denotes the imaginary-frequency-dependent HXC kernel at coupling strength α for the intersystem interaction. Similar to the Hartree kernel, the elements in the diagonal blocks of $\mathbf{K}_{\mathrm{int}}^{\alpha\mathrm{HXC}}(z)$ vanish, because $\boldsymbol{\Pi}^{0}(z)$ contains the full intra-fragment interaction.

Since $\mathbf{V}_{\mathrm{int}}$ and $\mathbf{K}_{\mathrm{int}}^{\alpha\mathrm{HXC}}$ have vanishing diagonal blocks, these can be used to further simplify the dispersion energy: Noting that the diagonal blocks of $\boldsymbol{\Pi}^{0}(z)\mathbf{V}_{\mathrm{int}}$ vanish, and using Eq. (17), the FDT (13) takes the form

$$E_{\mathrm{int}}^{\mathrm{C}}[\rho] = -\frac{1}{2}\int_{0}^{1} d\alpha \int_{-\infty}^{\infty} \frac{dz}{2\pi i} \left\langle \boldsymbol{\epsilon}^{\alpha}(z)^{-1}\boldsymbol{\Pi}^{0}(z)\mathbf{V}_{\mathrm{int}} \right\rangle. \tag{19}$$

For similar reasons, all even orders in the geometric series expansion of $\boldsymbol{\epsilon}^{\alpha}(z)^{-1}$ with respect to $\boldsymbol{\Pi}^{0}(z)\mathbf{K}_{\mathrm{int}}^{\alpha\mathrm{HXC}}(z)$ do not contribute to the dispersion energy. It is hence convenient to define the second-order generalized dielectric function

$$\boldsymbol{\kappa}^{\alpha}(z) = \boldsymbol{\epsilon}^{\alpha}(z)\left(\mathbf{2} - \boldsymbol{\epsilon}^{\alpha}(z)\right) = \mathbf{1} - \left(\boldsymbol{\Pi}^{0}(z)\mathbf{K}_{\mathrm{int}}^{\alpha\mathrm{HXC}}(z)\right)^{2}, \tag{20}$$

which is block diagonal with exponentially vanishing off-diagonal blocks. Substituting Eq. (20) into Eq. (19) and using the vanishing trace of $\boldsymbol{\kappa}^{\alpha}(z)^{-1}\boldsymbol{\Pi}^{0}(z)\mathbf{V}_{\mathrm{int}}$, we arrive at a central theoretical result of this paper,

$$E_{\mathrm{int}}^{\mathrm{C}}[\rho] = -\frac{1}{2}\int_{0}^{1} d\alpha \int_{-\infty}^{\infty} \frac{dz}{2\pi i} \left\langle \boldsymbol{\kappa}^{\alpha}(z)^{-1}\boldsymbol{\Pi}^{0}(z)\mathbf{K}_{\mathrm{int}}^{\alpha\mathrm{HXC}}(z)\boldsymbol{\Pi}^{0}(z)\mathbf{V}_{\mathrm{int}} \right\rangle. \tag{21}$$

Eq. (21) "exactifies" the well-known Longuet-Higgins Zaremba-Kohn[119,120] expression

for the second-order dispersion energy, denoted LHZK(2) in the following. Eq. (21) goes beyond LHZK(2) by including (i) exchange and correlation effects in the AB interaction through $\mathbf{K}_{\mathrm{int}}^{\alpha\mathrm{HXC}}$, and (ii) screening of the bare Coulomb interaction $\mathbf{V}_{\mathrm{int}}$ by $\boldsymbol{\kappa}^{\alpha}(i\omega)$. Indeed, the replacements $\mathbf{K}_{\mathrm{int}}^{\alpha\mathrm{HXC}} \to \alpha\mathbf{V}_{\mathrm{int}}$ and $\boldsymbol{\kappa}^{\alpha}(z) \to \mathbf{1}$ recover LHZK(2). Figure 4 displays a diagrammatic representation of Eq. (21).

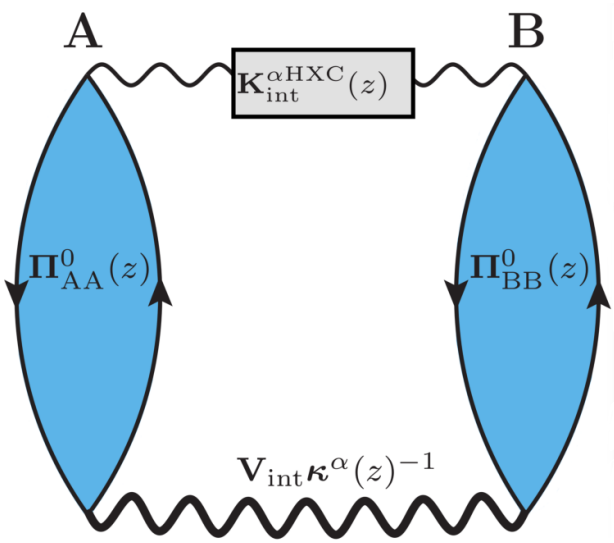

Figure 4: Diagrammatic representation of the A–B dispersion energy Eq. (21). Blue-shaded rings with upward–downward arrows denote particle–hole propagators of the monomers containing the full intra-monomer interaction, whereas horizontal wavy lines represent interactions between the monomers. Coupling strength and frequency integration are implied.

4.4 Convergence Radius of the AC-SAPT Series

The convergence of the AC-SAPT series, Eq. (6), is governed by the analyticity of the coupling strength integrand $W^{\alpha}[\rho]$ in the complex α plane: To guarantee convergence, the coupling strength integrand must be analytic for $|\alpha| \leq 1$. Using Eq. (19), this implies that $\boldsymbol{\epsilon}^{\alpha}(z)^{-1}$ must give rise to an analytic coupling strength integrand for $|\alpha| \leq 1$. A necessary condition for the latter is that $\boldsymbol{\epsilon}^{\alpha}(z)^{-1}$ is free of poles, i.e., by Eq. (17),

$$\left\|\boldsymbol{\Pi}^{0}(z)\mathbf{K}_{\mathrm{int}}^{\alpha\mathrm{HXC}}(z)\right\|_{2} = \left\|\mathbf{1} - \boldsymbol{\epsilon}^{\alpha}(z)\right\|_{2} < 1. \tag{22}$$

Here, the spectral norm $\|\cdot\|_2$ equals the largest singular value of an operator; $\|\cdot\|_2$ is induced by the scalar product on the tensor product space and thus a natural choice. An upper bound for the convergence radius of the AC-SAPT series is thus

$$\alpha_c = \min_{\alpha} \left\{ |\alpha| : \left\| \mathbf{\Pi}^0(z) \mathbf{K}_{\mathrm{int}}^{\alpha\mathrm{HXC}}(z) \right\|_2 = 1 \right\}. \tag{23}$$

α_c is generally an upper bound for the convergence radius, since $\boldsymbol{\epsilon}^\alpha(z)^{-1}$ could exhibit additional, non-algebraic singularities inside the complex α unit circle.

The convergence criterion (22) also implies that the geometric series

$$\boldsymbol{\kappa}^\alpha(z)^{-1} = \mathbf{1} + \left(\mathbf{\Pi}^0(z) \mathbf{K}_{\mathrm{int}}^{\alpha\mathrm{HXC}}(z) \right)^2 + \left(\mathbf{\Pi}^0(z) \mathbf{K}_{\mathrm{int}}^{\alpha\mathrm{HXC}}(z) \right)^4 + \ldots \tag{24}$$

converges, since, by the definition of the spectral norm and the negative definiteness of $\mathbf{\Pi}^0(z)$,

$$\left\| \mathbf{1} - \boldsymbol{\kappa}^\alpha(z) \right\|_2 = \left\| \left(\mathbf{\Pi}^0(z) \mathbf{K}_{\mathrm{int}}^{\alpha\mathrm{HXC}}(z) \right)^2 \right\|_2 = \left\| \mathbf{\Pi}^0(z) \mathbf{K}_{\mathrm{int}}^{\alpha\mathrm{HXC}}(z) \right\|_2^2 < 1. \tag{25}$$

Necessary conditions equivalent to Eq. (22) are thus that $\boldsymbol{\kappa}^\alpha(z)$ be positive definite or $\boldsymbol{\epsilon}^\alpha(z)^{-1}$ have eigenvalues < 2.

4.5 Approximations within AC-SAPT

In the following, we determine the asymptotic expressions for the dispersion energy corresponding to supermolecular RPA and MBPT calculations, and analyze the consequences for the AC-SAPT expansion.

4.5.1 Random Phase Approximation

The RPA polarization propagator at zero intermonomer interaction,

$$\mathbf{\Pi}^{\mathrm{RPA}}(z) = \left(\mathbf{1} - \mathbf{\Pi}_0^0(z) \mathbf{V}_0 \right)^{-1} \mathbf{\Pi}_0^0(z), \tag{26}$$

is defined in terms of the bare KS polarization propagator of the supersystem $\mathbf{\Pi}_0^0$, which does not include any electron-electron interactions, and the intramonomer interaction $\mathbf{V}_0$ with the matrix representation

$$\mathbf{V}_0 = \begin{pmatrix} \mathbf{V}_{AA} & \mathbf{0} \\ \mathbf{0} & \mathbf{V}_{BB} \end{pmatrix} \tag{27}$$

in the large R limit. A supermolecular RPA calculation corresponds to the replacements

$$\mathbf{K}_{\mathrm{int}}^{\alpha\mathrm{HXC}}(z) \to \alpha \mathbf{V}_{\mathrm{int}} \quad \text{and} \quad \mathbf{\Pi}^0(z) \to \mathbf{\Pi}^{\mathrm{RPA}}(z) \tag{28}$$

in Eqs. (13)-(23). In other words, the intramolecular electron correlation and the screening factor $\boldsymbol{\kappa}^{\alpha}(z)^{-1}$ in Eq. (21) are treated non-perturbatively, whereas the intermolecular HXC kernel is replaced by its first-order approximation.

Condition (22) implies that, within RPA, the AC-SAPT series will converge if

$$|\alpha| \left\| \mathbf{\Pi}^{\mathrm{RPA}}(z) \mathbf{V}_{\mathrm{int}} \right\|_2 < 1. \tag{29}$$

This condition is necessary and sufficient for RPA, because the only singularities of the RPA coupling strength integrand in the complex α plane result from zeros of

$$\boldsymbol{\kappa}^{\alpha\mathrm{RPA}}(z) = \mathbf{1} - \alpha^2 \left(\mathbf{\Pi}^{\mathrm{RPA}}(z) \mathbf{V}_{\mathrm{int}} \right)^2. \tag{30}$$

The convergence radius thus has the lower bound

$$\alpha_c^{\mathrm{RPA}} = \left\| \mathbf{\Pi}^{\mathrm{RPA}}(z) \mathbf{V}_{\mathrm{int}} \right\|_2^{-1} \geq \left\| \mathbf{\Pi}^{\mathrm{RPA}}(z) \mathbf{V}_0 \right\|_2^{-1} \left\| \mathbf{V}_0^{-1} \mathbf{V}_{\mathrm{int}} \right\|_2^{-1}, \tag{31}$$

where the inequality follows from the submultiplicativity of the spectral norm. Since $\mathbf{\Pi}^0(z)\mathbf{V}_0$ is negative definite,

$$\left\| \mathbf{\Pi}^{\mathrm{RPA}}(z) \mathbf{V}_0 \right\|_2 \leq 1 \tag{32}$$

by Eq. (26). Moreover, $\left\|\mathbf{V}_0^{-1}\mathbf{V}_{\rm int}\right\|_2 \leq 1$ follows[121] from the fact that both $\mathbf{V}_0$ and $\mathbf{V}_0+\mathbf{V}_{\rm int}$, corresponding to the monomer-only and supersystem Hartree kernels, are positive definite. Consequently,

$$\alpha_c^{\rm RPA} \geq 1, \tag{33}$$

where the inequality holds as long as $\left\|\mathbf{\Pi}_0^0(z)\mathbf{V}_0\right\|_2 < \infty$. This condition is satisfied for monomers with finite KS gap, where $\mathbf{\Pi}_0^0(z)$ is bounded, but may be violated, e.g., for infinite one-dimensional metals, see below. Hence, the AC-SAPT series always converges within RPA for nondegenerate monomers.

RPA permits analytic integration over coupling strength in Eq. (21), yielding a compact expression for the dispersion energy within RPA,

$$E_{\rm int}^{\rm C\ RPA}[\rho] = \frac{1}{4}\int_{-\infty}^{\infty}\frac{d\omega}{2\pi}\langle \ln \boldsymbol{\kappa}^{\rm RPA}(z)\rangle. \tag{34}$$

Eq. (34) illustrates how the analytic structure of $\ln \boldsymbol{\kappa}^{\rm RPA}(z)$ governs the convergence of the AC-SAPT expansion at full coupling within RPA. For nondegenerate monomers, $\boldsymbol{\kappa}^{\rm RPA}(z)$ is positive definite with eigenvalues between 0 and 1, and thus the Taylor expansion around $\boldsymbol{\kappa}^{\rm RPA}(z) = \mathbf{1}$, which generates the AC-SAPT series, converges. However, if $\boldsymbol{\kappa}^{\rm RPA}(z)$ has zero eigenvalues, the series diverges due to the essential singularity of the natural logarithm at zero.

Dobson and Gould (DG) obtained Eq. (34) by a coupling strength integration argument without density constraint, and showed that it reduces to the non-retarded Lifshitz formula for macroscopic slab systems, which is accurate for dispersion interactions between macroscopic objects.[2] DG also identified conditions for which Eq. (34) predicts unconventional power laws of dispersion interactions that cannot be obtained from AC-SAPT: Systems must be macroscopic in at least one dimension, allowing for infinite-wavelength density fluctuations, finite in at least one other dimension, and exhibit zero electronic gap. This is precisely when $\boldsymbol{\kappa}^{\rm RPA}(z)$ can have zero eigenvalues, causing AC-SAPT to diverge. The unconventional

power laws observed[52] for these systems cannot be obtained from a Taylor series with respect to α and thus are examples of physical systems exhibiting divergence of AC-SAPT.

4.5.2 Many-Body Perturbation Theory

In the present framework, supersystem MBPT calculations correspond to perturbatively expanding the coupling strength integrand $W^\alpha[\rho]$ with respect to both, the inter- and intra-monomer interaction, such that the resulting total interaction energy is consistent to a given finite order. In the following, we consider supersystem MBPT(2) theory, which is by far the most commonly used MBPT approach for NIs in large molecular systems. Supersystem MBPT(2) corresponds to the replacements

$$\mathbf{K}_{\mathrm{int}}^{\alpha\mathrm{HXC}}(z) \to \alpha\mathbf{V}_{\mathrm{int}} \quad \text{and} \quad \mathbf{\Pi}^0(z) \to \mathbf{\Pi}_0^0(z) \quad \text{and} \quad \boldsymbol{\kappa}_\alpha(z) \to \mathbf{1} \tag{35}$$

in Eqs. (13)-(23). These replacements are sufficient to make the coupling strength integrand correct to first order, corresponding to MBPT(2) for the (coupling strength integrated) correlation energy. In the present constant-density AC approach, this is equivalent to second-order Görling–Levy perturbation theory treatment of the supersystem; analogous considerations apply to MP2. The replacements (35) amount to the LHZK(2) limit. This implies that the geometric series (24) is truncated after the first term, which is likely to result in large errors unless the series converges very rapidly.

Within the MBPT(2) approximation to monomer correlation, the convergence radius of the AC-SAPT series is, according to Eq. (23),

$$\alpha_c^{\mathrm{PT2}} = \left\| \mathbf{\Pi}_0^0(z)\mathbf{V}_{\mathrm{int}} \right\|_2^{-1}. \tag{36}$$

However, unlike the RPA propagator, $\mathbf{\Pi}_0^0\mathbf{V}_{\mathrm{int}}$ is generally not bounded by 1, which may cause unphysical divergence of the series.

Since exchange effects vanish exponentially for large R, MBPT(2) coincides with the

second-order perturbative limit of RPA, enabling us to alternatively consider the behavior of the coupling-strength integrated AC-SAPT expansion within MBPT(2) via Eqs. (30) and (34). Clearly, this argument can only be used as long as RPA itself is reasonably accurate, a conclusion supported by our results. MBPT(2) corresponds to replacing $\boldsymbol{\kappa}^{\mathrm{RPA}}(z)$, the generalized second-order RPA dielectric function at full intra-monomer coupling with

$$\boldsymbol{\kappa}^{\mathrm{PT2}}(z) = \mathbf{1} - \left(\boldsymbol{\Pi}_0^0(z)\mathbf{V}\right)^2, \tag{37}$$

and truncating the Taylor expansion of $\ln \boldsymbol{\kappa}^{\mathrm{PT2}}(z)$ after the first order. However, since $\boldsymbol{\Pi}_0^0(z)$ is unbounded, $\boldsymbol{\kappa}^{\mathrm{PT2}}(z)$ may exhibit eigenvalues ≤ 0 even for finite, nondegenerate monomers, corresponding to nonanalytic behavior of $\ln \boldsymbol{\kappa}^{\mathrm{PT2}}(z)$. In this scenario, the Taylor expansion of the natural logarithm around $\boldsymbol{\kappa}^{\mathrm{PT2}}(z) = \mathbf{1}$ spuriously diverges, and the first-order approximation may be expected to yield a poor approximation to the RPA dispersion energy.

4.5.3 MP2C: Partial Resummation of MBPT

Heßelmann's MP2C method[45–47] replaces the (uncoupled) LHZK(2) part of the MP2 interaction energy with its (coupled) time-dependent DFT counterpart. In the large-R asymptotic limit, time-dependent DFT reduces to RPA, and hence MP2C corresponds to the replacements

$$\mathbf{K}_{\mathrm{int}}^{\alpha\mathrm{HXC}}(z) \to \alpha\mathbf{V}_{\mathrm{int}} \quad \text{and} \quad \boldsymbol{\Pi}^0(z) \to \boldsymbol{\Pi}^{\mathrm{RPA}}(z) \quad \text{and} \quad \boldsymbol{\kappa}_\alpha(z) \to \mathbf{1} \tag{38}$$

in Eqs. (13)-(23). Equivalently, MP2C may be understood as a low-order approximation to the RPA dispersion energy resulting from first-order truncation of the Taylor expansion of $\ln \boldsymbol{\kappa}^{\mathrm{RPA}}(z)$ in Eq. (34) around $\boldsymbol{\kappa}^{\mathrm{RPA}}(z) = \mathbf{1}$,

$$E_{\mathrm{int}}^{\mathrm{C\ PT2C}}[\rho] = \frac{1}{4}\int_{-\infty}^{\infty} \frac{d\omega}{2\pi} \langle \boldsymbol{\kappa}^{\mathrm{RPA}}(z) - \mathbf{1} \rangle. \tag{39}$$

In other words, MP2C includes intramonomer screening effects to infinite order, but the intermonomer interaction is second order only. The convergence of this partially resummed MBPT series is more benign compared to standard MBPT, because, for non-degenerate monomers, the eigenvalues of $\boldsymbol{\kappa}^{\mathrm{RPA}}(z)$ are between 0 and 1, and hence the Taylor expansion of $\ln \boldsymbol{\kappa}^{\mathrm{RPA}}(z)$ converges. Also, since $\ln x \leq x - 1$ for $0 < x \leq 1$, the MP2C dispersion energy is an upper bound for the RPA dispersion energy. However, with decreasing eigenvalues of $\boldsymbol{\kappa}^{\mathrm{RPA}}(z)$, i.e., for large and polarizable monomers, this Taylor series converges increasingly slowly (and eventually diverges under DG conditions), and hence this bound deteriorates rapidly. This is consistent with the observation that MP2C underestimates binding energies of larger complexes contained in the L7 benchmark.[68] Unlike the previously discussed RPA and MBPT approximations, the MP2C method does not possess a "seamless" supermolecular equivalent, i.e., it requires an SAPT-style partitioning into monomers, because the inter- and intramonomer interactions are treated at different levels. From a computational viewpoint, truncation of the Taylor expansion of $\ln \boldsymbol{\kappa}^{\mathrm{RPA}}(z)$ offers little advantage compared to full RPA using Eq. (34).

Fig. 5 summarizes the approximations to the AC-SAPT dispersion energy discussed in this section in diagrammatic form.

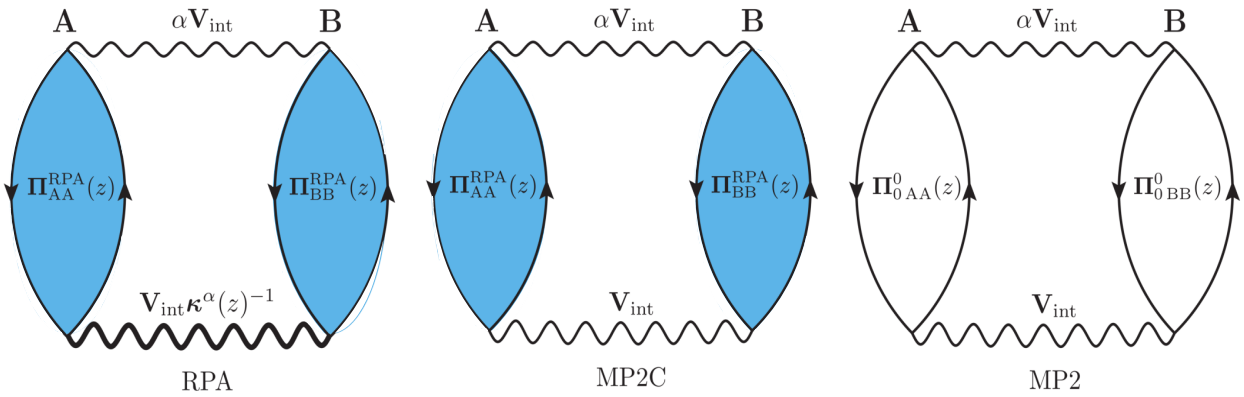

Figure 5: Diagrammatic representations of the A–B dispersion energy within RPA, MP2C, and MP2. Blue-shaded and empty rings with upward–downward arrows denote particle–hole propagators of the monomers containing the full and zero intra-monomer interaction, respectively, whereas horizontal wavy lines represent interactions between the monomers. Coupling strength and frequency integration are implied.

4.6 Numerical Validation

4.6.1 Convergence Estimates

The previous sections suggest that the AC-SAPT convergence radius α_c depends critically on the level of theory used to describe the monomers (through $\mathbf{\Pi}_0$). Here we numerically evaluate the upper bounds for α_c^{PT2} and investigate whether these asymptotic bounds can serve as meaningful convergence estimates for large but finite R.

Starting from Eq. (36) and using the same inequalities as in Sec. 4.5.1, we obtain

$$\alpha_c^{\mathrm{PT2}}(z) \geq \left\| \mathbf{\Pi}_0^0(z) \mathbf{V}_0 \right\|_2^{-1}. \tag{40}$$

Since the spectral norm is invariant under similarity transformations,

$$\left\| \mathbf{\Pi}_0^0(z) \mathbf{V}_0 \right\|_2 = \| \mathbf{Q}(z) \|_2, \tag{41}$$

where $\mathbf{Q}(z) = -\mathbf{L}^T \mathbf{\Pi}^0(z) \mathbf{L}$ and $\mathbf{L}$ is the Cholesky factor of $\mathbf{V}^0$. $\mathbf{Q}(z)$ is routinely computed in efficient RPA and beyond-RPA implementations.[64,65,122] For purely imaginary z, $\|\mathbf{Q}(z)\|_2$ has a maximum at $z = 0$ and is otherwise monotonous, as may be demonstrated, e.g., using the spectral representation of $\mathbf{\Pi}^0(z)$. Thus,

$$\alpha_c^{\mathrm{PT2}}(z) \geq \underline{\alpha}_c^{\mathrm{PT2}} = \| \mathbf{Q}(0) \|_2^{-1}. \tag{42}$$

Figure 6 shows the correlation between absolute errors in MP2 interaction energies and the inverse convergence radius $1/\underline{\alpha}_c^{\mathrm{PT2}}$, evaluated using a PBE KS reference. As long as $1/\underline{\alpha}_c^{\mathrm{PT2}}$ is close to 1, the MP2 errors are small, but they increase rapidly once $1/\underline{\alpha}_c^{\mathrm{PT2}}$ increases above ~ 3. The correlation is quite convincing since (i) divergence at α values close to 1 may not translate into large MP2 errors, (ii) a KS reference yields $1/\underline{\alpha}_c^{\mathrm{PT2}}$ values 2-3 times larger than a HF reference, see Fig 6. With decreasing convergence radius, MP2 and the

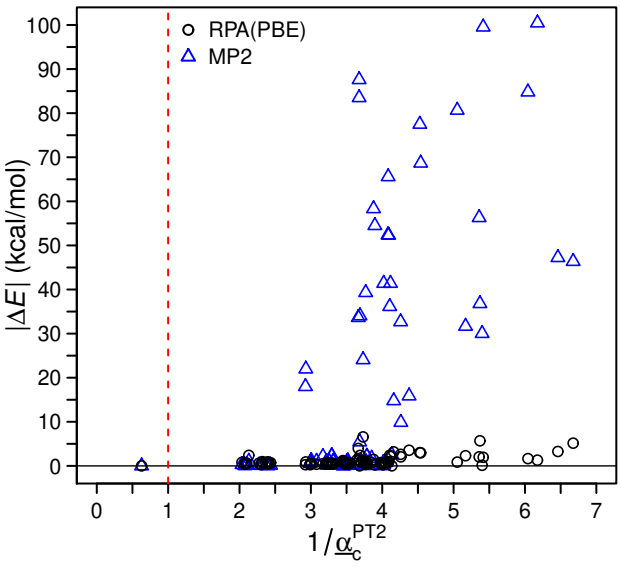

Figure 6: Absolute MP2 and RPA interaction energy errors $|\Delta E|$ for the S66,[66,67] L7,[68] and S30L[69] benchmarks as well as helium dimer as functions of the inverse convergence radius $1/\underline{\alpha}_c^{\mathrm{PT2}}$. $\underline{\alpha}_c^{\mathrm{PT2}}$ was evaluated using a PBE KS reference and cc-pVTZ basis sets.

LHZK(2) dispersion energy become increasingly incorrect estimates of the exact dispersion energy (8). Figure 6 also shows that the RPA interaction energies are uncorrelated with $\underline{\alpha}_c^{\mathrm{PT2}}$, as expected from the estimate (33).

The convergence behavior of the AC-SAPT expansion in relation to $\underline{\alpha}_c^{\mathrm{PT2}}$ is further illustrated by re-expansion of the RPA interaction energy in powers of α, see Figure 7. Only for helium dimer ($\underline{\alpha}_c^{\mathrm{PT2}} = 1.59$ with a PBE reference), the series converges with respect to the spectral norm. For all other cases, increasingly large oscillations are observed at higher orders. This behavior is characteristic of asymptotic series and has been observed for MBPT ground state energies.[28,123,124] With decreasing $\underline{\alpha}_c^{\mathrm{PT2}}$, the oscillations become more pronounced lower orders, causing significant error even at $n = 2$. While the convergence radii for some of the smaller systems are closer to 1 with a HF reference compared to a PBE reference, their AC-SAPT series eventually diverge as well.

In their 1993 work,[26] Moszynski, Jeziorski, and Szalewicz considered the convergence of MBPT supermolecular dispersion energies using a HF reference for He_2, $(H_2)_2$, $(LiH)_2$, $(H_2O)_2$, and $(HF)_2$ within the ring approximation, which is equivalent to RPA. Based on

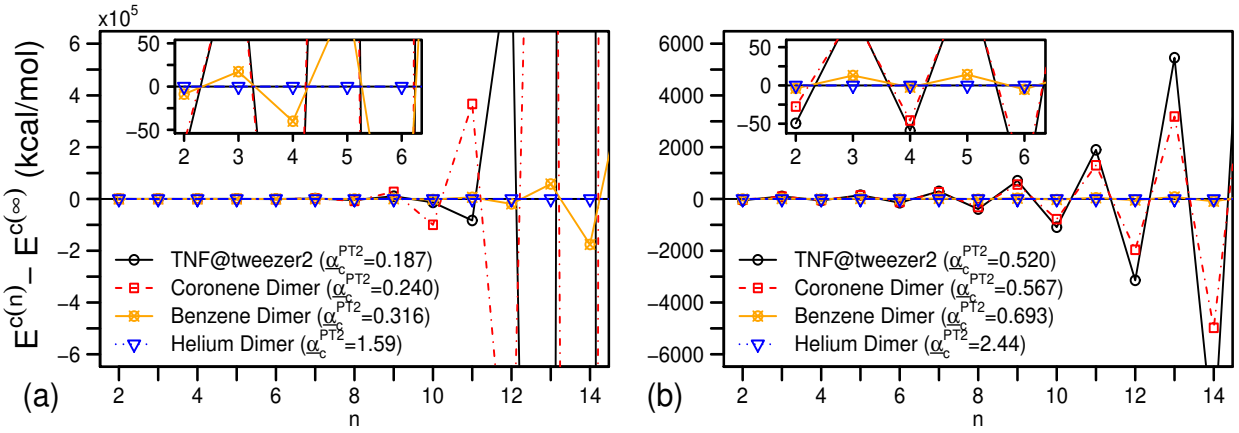

Figure 7: Errors (kcal/mol) of MBPT(n) interaction energies within the ring approximation (i.e. RPA) using (a) a KS and (b) a HF reference and cc-pVTZ basis sets. Insets show lower orders on a smaller energy scale.

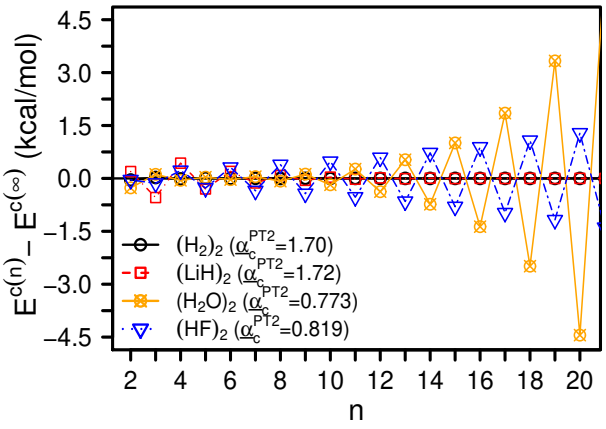

Figure 8: Errors (kcal/mol) of MBPT(n) interaction energies within the ring approximation (i.e. RPA) using a HF reference and cc-pVTZ basis sets for the dimers taken from Ref. 26.

numerical results up to order $n = 10$, they concluded that the convergence of the MBPT expansion for these systems is "very fast." While we confirm this conclusion for He_2, the present results suggest that the MBPT expansion of the dispersion energy indeed diverges for modestly larger systems. For example, our results for $(H_2O)_2$ agree well with those of Moszynski, Jeziorski, and Szalewicz up to $n = 10$, but the $\underline{\alpha}_c^{\mathrm{PT2}}$ value of 0.773 suggests that the series is divergent. Indeed, oscillations of increasing magnitude are observed when orders up to $n = 20$ are considered, see Figure 8.

4.6.2 Size Dependence of Errors

The dependence of the convergence radius estimate $\underline{\alpha}_c^{\mathrm{PT2}}$ on the size of the complex is displayed in Figure 9. Only for the helium dimer, $\underline{\alpha}_c^{\mathrm{PT2}} > 1$, whereas $\underline{\alpha}_c^{\mathrm{PT2}}$ is significantly smaller than 1 for all systems in the S66,[66,67] L7,[68] and S30L[69] benchmarks. Clearly, as opposed to $\mathbf{\Pi}_0^{\mathrm{RPA}}(0)$, $\mathbf{\Pi}^0(0)$ is not necessarily bounded. Whether $\|\mathbf{\Pi}^0(0)\mathbf{V}_{\mathrm{int}}\|_2$ saturates or becomes infinite in the thermodynamic limit is system-dependent; nevertheless, the convergence criterion Eq. (22) suggests that perturbative calculations of NIs start to diverge already for fairly small system sizes with few tens of atoms and comparatively large HOMO–LUMO gap. Indeed, the HOMO–LUMO gap is a fairly poor estimator of the interaction energy error, see Supporting Information.

Relative errors in NIs as a function of system size are shown in Figure 10. While the correlation of the errors with the number of valence electrons (VEs) is less strong than the one observed for the convergence estimates, there are clearly discernible trends: Whereas percentage errors in binding energies are virtually constant within RPA, they increase linearly for MP2, at a rate of approximately 0.1%, per VE on average. For slightly over 700 valence electrons, the MP2 relative error regression fit reaches 100% for the systems tested here. SCS-MP2 has an approximately 5 times lower slope of 0.025%, per VE (but notably higher y-intercept), and PBE-D3 relative errors grow at a rate of slightly less than 0.01%, for the present benchmarks, see Table 2. The largest MP2 errors occur for systems with strong π–π

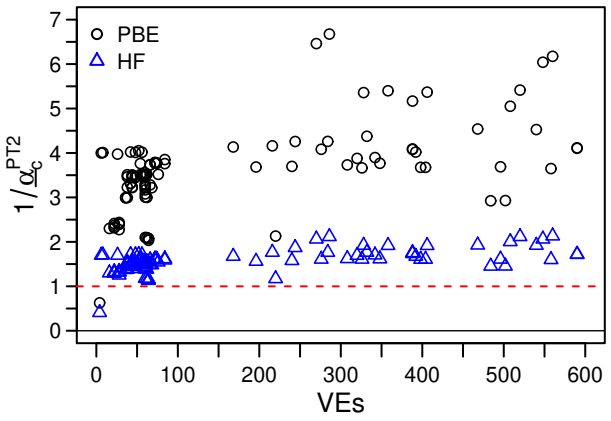

Figure 9: Inverse of the convergence radius ($1/\underline{\alpha}_c^{PT2}$) for MBPT(2) with PBE and HF references vs. number of valence electrons (VEs) for the S66,[66,67] L7,[68] and S30L[69] benchmarks, and helium dimer. $\underline{\alpha}_c^{PT2}$ values were computed using cc-pVTZ basis sets. A $1/\underline{\alpha}_c^{PT2}$ value ≥ 1 indicates divergence of the AC-SAPT series.

stacking interactions such as complexes 3 to 12 from the S30L test set.[69]

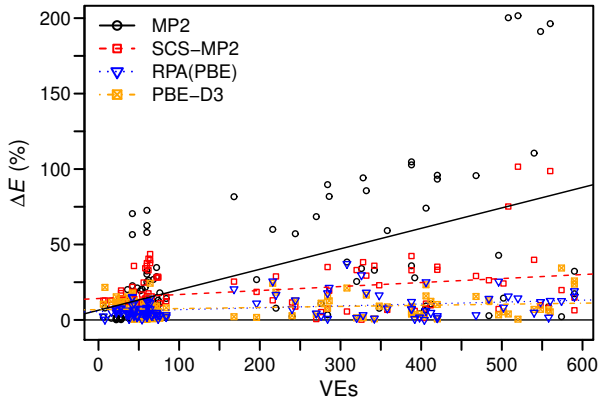

Figure 10: Relative errors (ΔE) of MP2, SCS-MP2, RPA(PBE), and PBE-D3 interaction energies in the S66,[66,67] L7,[68] and S30L[69] benchmarks vs. number of valence electrons (VEs).

4.7 Physical Interpretation

The present analytical and numerical results show that the convergence of the AC-SAPT series for NIs is strongly dependent on the level of theory used for computing the monomer polarization propagator $\mathbf{\Pi}^0(z)$. Thus, it is helpful to consider the generalized dielectric

Table 2: Parameters of the linear regression fits displayed in Figure 10. The slope corresponds to the average relative interaction energy error (%) per valence electron (VE), and the y-intercept corresponds to the average relative interaction energy error (%) in the limit of zero VEs.

Method	Slope (%/VE)	y-intercept (%)
MP2	0.1219	7.30
SCS-MP2	0.0251	14.10
RPA(PBE)	0.0030	6.24
PBE-D3	0.0083	6.79

function

$$\boldsymbol{\epsilon}_0(z) = \mathbf{1} - \boldsymbol{\Pi}^0(z)\mathbf{V}_0, \tag{43}$$

which characterizes the response of the monomers at frequency z. Within RPA, Eq. (32) implies that the eigenvalues of $\boldsymbol{\epsilon}_0$ are bounded from above by 2, reflecting the fact that the RPA response to external fields is reduced ("screened") by the creation of induced electron-pairs. As a result, the effective interaction "seen" by an electron of subsystem A due to electrons in subsystem B decays rapidly within B. This effective interaction is indeed "weak" in the sense that it affords a convergent AC-SAPT expansion for nondegenerate monomers.

For systems satisfying the DG conditions, there is no screening in the monomers in at least one dimension, and the largest eigenvalue of $\boldsymbol{\epsilon}_0(z)$ may equal 2, even within RPA, causing divergence of the AC-SAPT expansion and unconventional power laws of the dispersion interaction. Since the HXC kernel is dominated by the Hartree kernel for large R, this behavior of the RPA is expected to be correct, at least qualitatively.

As opposed to these physical divergences of the AC-SAPT expansion, unphysical divergences may result if the intra-monomer electron interaction is treated perturbatively. In this case, $\boldsymbol{\epsilon}_0$ is not bounded, with largest eigenvalues around 5 (KS reference) or 2 (HF reference) for typical systems studied here, see Figures 6 and 9. This reflects a much stronger perturbation of the monomers by the intersystem interaction due to incomplete screening resulting primarily from the neglect of higher-order particle–hole ring diagrams. Hence, the MBPT effective interaction is too strong for intermolecular perturbation theory, causing

spurious divergence of the AC-SAPT expansion. This effect is not seen in the smallest and least polarizable monomers such as He atoms, but it becomes noticeable for even moderately large monomers with a few atoms, where the neglect of screening due to multiple induced particle–hole pairs by finite-order MBPT produces significant over- or underestimations of NIs. For the large π systems in the S30L, the lack of screening produces maximum eigenvalues of $\boldsymbol{\epsilon}_0$ around 7 (KS reference) or 3 (HF reference), which suggests rapid divergence of the AC-SAPT expansion, providing a plausible rationale for the spectacular errors in MP2 binding energies observed for these systems.

5 Conclusions

A key result of this study is that dispersion interactions cannot be considered "weak" unless intra-monomer screening effects are taken into account at least at the level of RPA. Similar to electrostatic screening, electrodynamic screening due to induced density fluctuations is inadequately captured by finite-order MBPT-type approaches, except for the smallest and least polarizable systems. As a result, unscreened perturbation theories produce exaggerated responses of the monomers to external perturbation and divergent estimates for NIs even in moderately large systems. The conventional wisdom that MBPT is useful for accurate calculations of NIs in even moderately large systems is incorrect: Numerically small interaction energies compared to covalent interactions do not imply "weakness" in the sense of a bounded response or convergent intermolecular perturbation theory. Consequently, finite-order MBPT results tend to worsen systematically with system size, as was demonstrated by the basis-set extrapolated MP2 results for complexes with up to 600 VEs. Given the computational efficiency and popularity of MBPT implementations, this is a sobering result: Size-extensivity and (conventional) size-consistency are insufficient conditions for accurate predictions of NIs. While there may be a place for MBPT calculations of NIs in complexes of small, hard monomers, MBPT estimates of NIs cannot be considered reliable for most

systems of chemical interest, much less for nanomaterials, metallic systems, or soft matter. In light of the current results, empirically scaled MP2 methods, and particularly MP2.5, appear as simple regularizations of an asymptotic series; while this strategy is clearly successful for some systems, it does not address the underlying physical problem, limiting predictive power and robustness.

The MP2C method can be viewed as a partial MBPT resummation which includes intra-monomer screening and exhibits better analytical properties than bare MBPT, but truncates intermonomer interactions at second order, and has no obvious supermolecular equivalent. For increasingly large and polarizable monomers, MP2C underestimates the magnitude of dispersion interactions progressively due to missing many-body dispersion.

A qualitatively correct treatment of intra-monomer screening to all orders is possible with RPA at little extra cost compared to MBPT approaches. Indeed, RPA produces constant relative errors in NIs that are virtually independent of the system size and type, consistent with its qualitatively correct treatment of electrodynamic polarization; this may be viewed as a manifestation of "Casimir-Polder size consistency."[125] Similar conclusions may hold for more elaborate non-perturbative coupled cluster methods, which include the ring diagrams corresponding to RPA.[126] In particular, the accuracy of ring-coupled-cluster methods for NIs[127] supports the view that ring diagrams dominate in the long-range limit of NIs. It is remarkable that ring diagrams also constitute the main part of the correlation energy for the uniform electron gas at high density,[57] a similarity first noted by Dzyaloshinskii, Lifshitz, and Pitaevskii.[128] Both, dispersion interactions in finite systems and electron correlation in the high-density electron gas emerge from collective density fluctuations[129,130] caused by the long-range Coulomb interaction. In this sense, the expectation that RPA energy differences should be universally accurate[131,132] appears to hold as long as long-range correlation dominates.

The present results raise the question whether the perturbative triples correction of CCSD(T) inherits any of the limitations of MBPT, even though it includes some screening at the level of the amplitudes. Whereas CCSD(T) errors for interaction energies of small

molecular complexes were determined to be on the order of 1%,[68] and typical deviations between RPA and CCSD(T) binding energies are on the order of 5-10% for the benchmarks studied here, the linear scaling domain-based pair natural orbital CCSD(T) binding energies for water on small graphene flakes are significantly larger than the corresponding RPA and diffusion Monte Carlo ones,[133] and the CCSD(T) perturbative triples correction diverges for the correlation energy of the uniform electron gas.[134]

The AC-SAPT formalism developed here affords separate, non-perturbative definitions of dispersion and induction effects in NIs. While it has mainly been used to rationalize the results of supermolecular calculations here, the analytical expressions obtained from AC-SAPT could be evaluated using monomer calculations given suitable approximations to the intermolecular KS potential $\hat{V}_{s\,\mathrm{int}}[\rho]$. Beyond-RPA perturbation methods known from supermolecular calculations such as second-order screened exchange (SOSEX)[63,135–137] or approximate exchange kernel (AXK)[122,138] may prove useful for this purpose. Our conclusions regarding the divergence of MBPT for NIs rely in part on the assumption that the RPA dispersion energy is qualitatively accurate, which is supported by the close agreement between the RPA and the benchmark results. This agreement is remarkable given that RPA is parameter-free aside from using a KS reference from a semilocal DFA. Moreover, the estimated AC-SAPT convergence radii are upper bounds only, but they show strong correlation to the NI errors of MBPT methods for the benchmarks studied here.

Our results show that the convergence of the AC-SAPT expansion for dimers consisting of large monomers depends critically on the accuracy of intra-monomer correlation. Specifically, electrodynamic screening should be included in the monomer correlation treatment at least at the time-dependent HF level. Apart from unphysical divergences, AC-SAPT does converge more slowly for large and polarizable monomers, and exhibits physical divergence for systems satisfying the DG conditions such as one-dimensional metals. Under these circumstances, the traditional LHZK(2) picture of dispersion breaks down and must replaced by the RPA one embodied in Eq. (34). Importantly, Eq. (34) correctly recovers both, the small, hard

monomer LHZK(2) limit where MBPT can converge, and the macroscopic Lifshitz limit. Eq. (34) is largely scale invariant and therefore a far better starting point for computing and conceptualizing dispersion interactions than LHZK(2).

The breakdown of MBPT for NIs also has important implications for the development of approximations such as van-der-Waals density functionals or force fields. The present results cast further doubt on the validity of empirical $1/R^6$ corrections for very large and polarizable monomers – even though some dispersion-corrected DFAs admittedly perform remarkably well for large systems. An accurate description of NIs for such systems may require methods including Lifshitz-type physics and electrodynamic polarization effects. Quantum Drude models[139] or many-body dispersion methods[51,140] may be considered coarse-grained RPA approaches suitable for this purpose.

Modern RPA implementations are insignificantly more expensive than the most advanced MP2 approaches from a computational viewpoint, and RPA calculations for molecules with hundreds of atoms on workstation clusters are now routine[64,98,141–147] — although the present results also show that accurate RPA binding energies for NIs require triple- to quadruple-ζ basis set extrapolation, making some of the proposed low-scaling methods less effective. Taken together with the superior accuracy of RPA for large and polarizable systems without empirical adjustments, MP2 can be safely and efficiently replaced by RPA for calculations of NIs in most systems of chemical interest. If MP2 results are nevertheless desired, diagnostic $\underline{\alpha}_c^{\mathrm{PT2}}$ values should be used to gauge their reliability. Similarly, the present results support the use of RPA calculations to calibrate dispersion-corrected DFA results.

RPA calculations of NIs benefit from variational optimization of the reference,[148] but the improvement appears to be most pronounced for small systems such as rare gas dimers and diminish with increasing monomer size. With average interaction energy errors consistently in the 5–10% range, RPA is accurate enough for a wide range of applications, irrespective of system size, gap size, or empirical training sets. The accuracy of RPA for NIs may also contribute to its recent successful application to activation energies of sterically crowded

transition states.[15,149]

Acknowledgement

This material is based upon work supported by the National Science Foundation under CHE-1464828 and CHE-1800431.

The authors declare the following competing financial interest(s): Principal investigator Filipp Furche has an equity interest in Turbomole GmbH. The terms of this arrangement have been reviewed and approved by the University of California, Irvine, in accordance with its conflict of interest policies.

Supporting Information Available

A listing of the contents of each file supplied as Supporting Information should be included. For instructions on what should be included in the Supporting Information as well as how to prepare this material for publications, refer to the journal's Instructions for Authors.

The following files are available free of charge:

- si.pdf: Total energies for the L7, S30L, and S66 benchmarks, complete ROT34 results, and further details and results

This material is available free of charge via the Internet at `http://pubs.acs.org/`.

References

(1) Hobza, P.; Zahradník, R.; Müller-Dethlefs, K. The World of Non-Covalent Interactions: 2006. *Collect. Czech. Chem. Commun.* **2006**, *71*, 443–531.

(2) Dobson, J. F.; Gould, T. Calculation of dispersion energies. *J. Phys.: Condens. Matter* **2012**, *24*, 073201.

(3) Dobson, J. F. Beyond pairwise additivity in London dispersion interactions. *Int. J. Quantum Chem.* **2014**, *114*, 1157–1161.

(4) Axilrod, B. M.; Teller, E. Interaction of the van der Waals Type Between Three Atoms. *J. Chem. Phys.* **1943**, *11*, 299–300.

(5) Muto, Y. Force between nonpolar molecules. *J. Phys. Math. Soc. Jpn* **1943**, *17*, 629–631.

(6) Huang, Z.; Qin, K.; Deng, G.; Wu, G.; Bai, Y.; Xu, J.; Wang, Z.; Yu, Z.; Scherman, O. A.; Zhang, X. Supramolecular Chemistry of Cucurbiturils: Tuning Cooperativity with Multiple Noncovalent Interactions from Positive to Negative. *Langmuir* **2016**, *32*, 12352 – 12360.

(7) Biedermann, F.; Schneider, H.-J. Experimental Binding Energies in Supramolecular Complexes. *Chem. Rev.* **2016**, *116*, 5216–5300.

(8) Britz, D. A.; Khlobystov, A. N. Noncovalent interactions of molecules with single walled carbon nanotubes. *Chem. Soc. Rev.* **2006**, *35*, 637–659.

(9) Liu, K.; Kang, Y.; Wang, Z.; Zhang, X. 25th anniversary article: reversible and adaptive functional supramolecular materials: ''noncovalent interaction'' matters. *Adv. Mater.* **2013**, *25*, 5530–5548.

(10) Georgakilas, V.; Tiwari, J. N.; Kemp, K. C.; Perman, J. A.; Bourlinos, A. B.; Kim, K. S.; Zboril, R. Noncovalent Functionalization of Graphene and Graphene Oxide for Energy Materials, Biosensing, Catalytic, and Biomedical Applications. *Chem. Rev.* **2016**, *116*, 5464–5519.

(11) Moulton, B.; Zaworotko, M. J. From Molecules to Crystal Engineering: Supramolecular Isomerism and Polymorphism in Network Solids. *Chem. Rev.* **2001**, *101*, 1629–1658.

(12) Beran, G. J. O. Modeling Polymorphic Molecular Crystals with Electronic Structure Theory. *Chem. Rev.* **2016**, *116*, 5567–5613.

(13) Becucci, M.; Melandri, S. High-Resolution Spectroscopic Studies of Complexes Formed by Medium-Size Organic Molecules. *Chem. Rev.* **2016**, *116*, 5014–5037.

(14) Zuend, S.; Jacobsen, E. N. Mechanism of Amido-Thiourea Catalyzed Enantioselective Imine Hydrocyanation: Transition State Stabilization via Multiple Non-Covalent Interactions. *J. Am. Chem. Soc.* **2009**, *131*, 15358–15374.

(15) Tao, D. J.; Muuronen, M.; Slutskyy, Y.; Le, A.; Furche, F.; Overman, L. E. Diastereoselective Coupling of Chiral Acetonide Trisubstituted Radicals with Alkenes. *Chem. Eur. J.* **2016**, *22*, 8786–8790.

(16) Pople, J. A.; Binkley, J. S.; Seeger, R. Theoretical models incorporating electron correlation. *Int. J. Quantum Chem.* **1976**, *10*, 1–19.

(17) Bartlett, R. J. Many-Body Perturbation Theory and Coupled Cluster Theory for Electron Correlation in Molecules. *Annu. Rev. Phys. Chem.* **1981**, *32*, 359–401.

(18) Hirata, S. Thermodynamic limit and size-consistent design. *Theor. Chem. Acc.* **2011**, *129*, 727–746.

(19) Møller, C.; Plesset, M. S. Note on an Approximation Treatment for Many-Electron Systems. *Phys. Rev.* **1934**, *46*, 618–622.

(20) Kristyán, S.; Pulay, P. Can (semi)local density functional theory account for the London dispersion forces? *Chem. Phys. Lett.* **1994**, *229*, 175–180.

(21) Pérez-Jordá, J.; Becke, A. D. A density-functional study of van der Waals forces: rare gas diatomics. *Chem. Phys. Lett.* **1995**, *233*, 134 – 137.

(22) Hobza, P.; Šponer, J.; Reschel, T. Density functional theory and molecular clusters. *J. Comput. Chem.* **1995**, *16*, 1315–1325.

(23) Antony, J.; Grimme, S. Is Spin-Component Scaled Second-Order Møller–Plesset Perturbation Theory an Appropriate Method for the Study of Noncovalent Interactions in Molecules? *J. Phys. Chem. A* **2007**, *111*, 4862–4868.

(24) Pitoňák, M.; Neogrády, P.; Černý, J.; Grimme, S.; Hobza, P. Scaled MP3 Non-Covalent Interaction Energies Agree Closely with Accurate CCSD(T) Benchmark Data. *ChemPhysChem* **2009**, *10*, 282–289.

(25) Riley, K. E.; Platts, J. A.; Řezáč, J.; Hobza, P.; Hill, J. G. Assessment of the Performance of MP2 and MP2 Variants for the Treatment of Noncovalent Interactions. *J. Phys. Chem. A* **2012**, *116*, 4159–4169.

(26) Moszynski, R.; Jeziorski, B.; Szalewicz, K. Møller–Plesset expansion of the dispersion energy in the ring approximation. *Int. J. Quantum Chem.* **1993**, *45*, 409–431.

(27) Moszynski, R.; Jeziorski, B.; Ratkiewicz, A.; Rybak, S. Many-body perturbation theory of electrostatic interactions between molecules: Comparison with full configuration interaction for four-electron dimers. *J. Chem. Phys.* **1993**, *99*, 8856–8869.

(28) Olsen, J.; Christiansen, O.; Koch, H.; Jørgensen, P. Surprising cases of divergent behavior in Møller–Plesset perturbation theory. *J. Chem. Phys.* **1996**, *105*, 5082–5090.

(29) Cremer, D.; He, Z. Sixth-Order Møller–Plesset Perturbation Theory–On the Convergence of the MPn Series. *J. Phys. Chem.* **1996**, *100*, 6173–6188.

(30) Leininger, M. L.; Allen, W. D.; Schaefer, H. F.; Sherrill, C. D. Is Mo/ller–Plesset perturbation theory a convergent ab initio method? *J. Chem. Phys.* **2000**, *112*, 9213–9222.

(31) Werner, H.-J. Eliminating the domain error in local explicitly correlated second-order Møller–Plesset perturbation theory. *J. Chem. Phys.* **2008**, *129*, 101103.

(32) Pulay, P. Localizability of dynamic electron correlation. *Chem. Phys. Lett.* **1983**, *100*, 151 – 154.

(33) Schütz, M.; Hetzer, G.; Werner, H.-J. Low-order scaling local electron correlation methods. I. Linear scaling local MP2. *J. Chem. Phys.* **1999**, *111*, 5691–5705.

(34) Manzer, S.; Horn, P. R.; Mardirossian, N.; Head-Gordon, M. Fast, accurate evaluation of exact exchange: The occ-RI-K algorithm. *J. Chem. Phys.* **2015**, *143*, 024113.

(35) Koch, H.; Sánchez de Merás, A.; Pedersen, T. B. Reduced scaling in electronic structure calculations using Cholesky decompositions. *J. Chem. Phys.* **2003**, *118*, 9481–9484.

(36) Witte, J.; Mardirossian, N.; Neaton, J. B.; Head-Gordon, M. Assessing DFT-D3 Damping Functions Across Widely Used Density Functionals: Can We Do Better? *J. Chem. Theory Comput.* **2017**, *13*, 2043–2052.

(37) Hohenstein, E. G.; Sherrill, C. D. Wavefunction methods for noncovalent interactions. *Wiley Interdiscip. Rev.: Comput. Mol. Sci.* **2012**, *2*, 304–326.

(38) Janowski, T.; Ford, A. R.; Pulay, P. Accurate correlated calculation of the intermolecular potential surface in the coronene dimer. *Mol. Phys.* **2010**, *108*, 249–257.

(39) Janowski, T.; Pulay, P. A benchmark quantum chemical study of the stacking interaction between larger polycondensed aromatic hydrocarbons. *Theo. Chem. Acc.* **2011**, *130*, 419–427.

(40) Grimme, S. Semiempirical GGA-type density functional constructed with a long-range dispersion correction. *J. Comput. Chem.* **2006**, *27*, 1787–1799.

(41) Grimme, S.; Antony, J.; Ehrlich, S.; Krieg, H. A consistent and accurate ab initio parametrization of density functional dispersion correction (DFT-D) for the 94 elements H-Pu. *J. Chem. Phys.* **2010**, *132*, 154104.

(42) Grimme, S. Supramolecular binding thermodynamics by dispersion-corrected density functional theory. *Chem. Eur. J.* **2012**, *18*, 9955–9964.

(43) Grimme, S. Improved Second-Order Møller–Plesset Perturbation Theory by Separate Scaling of Parallel- and Antiparallel-Spin Pair Correlation Energies. *J. Chem. Phys.* **2003**, *118*, 9095.

(44) Jung, Y.; Lochan, R. C.; Dutoi, A. D.; Head-Gordon, M. Scaled opposite-spin second order Møller–Plesset correlation energy: An economical electronic structure method. *J. Chem. Phys.* **2004**, *121*, 9793–9802.

(45) Heßelmann, A. Improved supermolecular second order Møller-Plesset intermolecular interaction energies using time-dependent density functional response theory. *J. Chem. Phys.* **2008**, *128*, 144112.

(46) Pitoňák, M.; Heßelmann, A. Accurate Intermolecular Interaction Energies from a Combination of MP2 and TDDFT Response Theory. *J. Chem. Theory Comput.* **2010**, *6*, 168–178.

(47) Huang, Y.; Shao, Y.; Beran, G. J. O. Accelerating MP2C dispersion corrections for dimers and molecular crystals. *J. Chem. Phys.* **2013**, *138*, 224112.

(48) Řezáč, J.; Greenwell, C.; Beran, G. J. O. Accurate Noncovalent Interactions via Dispersion-Corrected Second-Order Møller-Plesset Perturbation Theory. *J. Chem. Theory Comput.* **2018**, *14*, 4711–4721.

(49) Greenwell, C.; McKinley, J. L.; Zhang, P.; Zeng, Q.; Sun, G.; Li, B.; Wen, S.; Beran, G. J. O. Overcoming the difficulties of predicting conformational polymorph energetics in molecular crystals via correlated wavefunction methods. *Chem. Sci.* **2020**, –.

(50) Caldeweyher, E.; Bannwarth, C.; Grimme, S. Extension of the D3 dispersion coefficient model. *J. Chem. Phys.* **2017**, *147*, 034112.

(51) Tkatchenko, A.; DiStasio, R. A. J.; Car, R.; Scheffler, M. Accurate and efficient method for many-body van der Waals interactions. *Phys. Rev. Lett.* **2012**, *108*, 236402.

(52) Dobson, J. F.; White, A.; Rubio, A. Asymptotics of the Dispersion Interaction: Analytic Benchmarks for van der Waals Energy Functionals. *Phys. Rev. Lett.* **2006**, *96*, 073201.

(53) Lebègue, S.; Harl, J.; Gould, T.; Ángyán, J. G.; Kresse, G.; Dobson, J. F. Cohesive properties and asymptotics of the dispersion interaction in graphite by the random phase approximation. *Phys. Rev. Lett.* **2010**, *105*, 196401.

(54) Langreth, D. C.; Perdew, J. P. The Exchange-Correlation Energy of a Metallic Surface. *Solid State Commun.* **1975**, *17*, 1425–1429.

(55) Langreth, D. C.; Perdew, J. P. Exchange-Correlation Energy of a Metallic Surface: Wave-Vector Analysis. *Phys. Rev. B* **1977**, *15*, 2884–2901.

(56) Hult, E.; Rydberg, H.; Lundqvist, B. I.; Langreth, D. C. Unified treatment of asymptotic van der Waals forces. *Phys. Rev. B* **1999**, *59*, 4708–4713.

(57) Gell-Mann, M.; Brueckner, K. A. Correlation Energy of an Electron Gas at High Density. *Phys. Rev.* **1957**, *106*, 364–368.

(58) Dobson, J. F.; Wang, J.; Dinte, B. P.; McLennan, K.; Le, H. M. Soft cohesive forces. *Int. J. Quantum Chem.* **2005**, *101*, 579–598.

(59) Eshuis, H.; Furche, F. A Parameter-Free Density Functional That Works for Noncovalent Interactions. *J. Phys. Chem. Lett.* **2011**, *2*, 983–989.

(60) Lu, D.; Nguyen, H.-V.; Galli, G. Power series expansion of the random phase approximation correlation energy: The role of the third- and higher-order contributions. *J. Chem. Phys.* **2010**, *133*, 154110.

(61) Harl, J.; Kresse, G. Accurate bulk properties from approximate many-body techniques. *Phys. Rev. Lett.* **2009**, *103*, 056401.

(62) Heßelmann, A. In *Non-Covalent Interactions in Quantum Chemistry and Physics*; de la Roza, A. O., DiLabio, G. A., Eds.; Elsevier, 2017; pp 65 – 136.

(63) Beuerle, M.; Graf, D.; Schurkus, H. F.; Ochsenfeld, C. Efficient calculation of beyond RPA correlation energies in the dielectric matrix formalism. *J. Chem. Phys.* **2018**, *148*, 204104.

(64) Eshuis, H.; Yarkony, J.; Furche, F. Fast computation of molecular random phase approximation correlation energies using resolution of the identity and imaginary frequency integration. *J. Chem. Phys.* **2010**, *132*, 234114.

(65) Burow, A. M.; Bates, J. E.; Furche, F.; Eshuis, H. Analytical First-Order Molecular Properties and Forces within the Adiabatic Connection Random Phase Approximation. *J. Chem. Theory Comput.* **2014**, *10*, 180–194.

(66) Řezáč, J.; Riley, K. E.; Hobza, P. S66: A Well-balanced Database of Benchmark Interaction Energies Relevant to Biomolecular Structures. *J. Chem. Theory Comput.* **2011**, *7*, 2427–2438.

(67) Řezáč, J.; Riley, K. E.; Hobza, P. Extensions of the S66 Data Set: More Accurate Interaction Energies and Angular-Displaced Nonequilibrium Geometries. *J. Chem. Theory Comput.* **2011**, *7*, 3466–3470.

(68) Sedlak, R.; Janowski, T.; Pitoňák, M.; Řezáč, J.; Pulay, P.; Hobza, P. Accuracy of Quantum Chemical Methods for Large Noncovalent Complexes. *J. Chem. Theory Comput.* **2013**, *9*, 3364–3374.

(69) Sure, R.; Grimme, S. Comprehensive Benchmark of Association (Free) Energies of Realistic Host-Guest Complexes. *J. Chem. Theory Comput.* **2015**, *11*, 3785–3801.

(70) Grimme, S.; Steinmetz, M. Effects of London dispersion correction in density functional theory on the structures of organic molecules in the gas phase. *Phys. Chem. Chem. Phys.* **2013**, *15*, 16031–16042.

(71) Risthaus, T.; Steinmetz, M.; Grimme, S. Implementation of nuclear gradients of range-separated hybrid density functionals and benchmarking on rotational constants for organic molecules. *J. Comput. Chem.* **2014**, *35*, 1509–1516.

(72) Szalewicz, K.; Jeziorski, B. Symmetry-adapted double-perturbation analysis of intramolecular correlation effects in weak intermolecular interactions. *Mol. Phys.* **1979**, *38*, 191–208.

(73) Rybak, S.; Jeziorski, B.; Szalewicz, K. Many-body symmetry-adapted perturbation theory of intermolecular interactions. H_2O and HF dimers. *J. Chem. Phys.* **1991**, *95*, 6576–6601.

(74) Gunnarsson, O.; Lundqvist, B. I. Exchange and correlation in atoms, molecules, and solids by the spin-density-functional formalism. *Phys. Rev. B* **1976**, *13*, 4274–4298.

(75) Gunnarsson, O.; Lundqvist, B. I. Erratum: Exchange and correlation in atoms, molecules, and solids by the spin-density-functional formalism. *Phys. Rev. B* **1977**, *15*, 6006–6006.

(76) Hättig, C.; Hellweg, A.; Köhn, A. Distributed memory parallel implementation of energies and gradients for second-order Møller–Plesset perturbation theory with the resolution-of-the-identity approximation. *Phys. Chem. Chem. Phys.* **2006**, *8*, 1159–1169.

(77) Furche, F.; Ahlrichs, R.; Hättig, C.; Klopper, W.; Sierka, M.; Weigend, F. Turbomole. *WIREs Comput. Mol. Sci.* **2014**, *4*, 91–100.

(78) Perdew, J. P.; Burke, K.; Ernzerhof, M. Generalized Gradient Approximation Made Simple. *Phys. Rev. Lett.* **1996**, *77*, 3865–3868.

(79) Tao, J.; Perdew, J.; Staroverov, V.; Scuseria, G. Climbing the Density Functional Ladder: Nonempirical Meta-Generalized Gradient Approximation Designed for Molecules and Solids. *Phys. Rev. Lett.* **2003**, *91*, 146401.

(80) Treutler, O.; Ahlrichs, R. Efficient molecular numerical integration schemes. *J. Chem. Phys.* **1995**, *102*, 346.

(81) Caldeweyher, E.; Ehlert, S.; Hansen, A.; Neugebauer, H.; Spicher, S.; Bannwarth, C.; Grimme, S. A generally applicable atomic-charge dependent London dispersion correction. *J. Chem. Phys.* **2019**, *150*, 154122.

(82) Brandenburg, J. G.; Bannwarth, C.; Hansen, A.; Grimme, S. B97–3c: A revised low-cost variant of the B97–D density functional method. *J. Chem. Phys.* **2018**, *148*, 064104.

(83) Liakos, D. G.; Sparta, M.; Kesharwani, M. K.; Martin, J. M. L.; Neese, F. Exploring the Accuracy Limits of Local Pair Natural Orbital Coupled-Cluster Theory. *J. Chem. Theory Comput.* **2015**, *11*, 1525–1539.

(84) Carter-Fenk, K.; Lao, K. U.; Liu, K.-Y.; Herbert, J. M. Accurate and Efficient ab Initio Calculations for Supramolecular Complexes: Symmetry-Adapted Perturbation Theory with Many-Body Dispersion. *J. Phys. Chem. Lett.* **2019**, *10*, 2706–2714.

(85) Kruse, H.; Mladek, A.; Gkionis, K.; Hansen, A.; Grimme, S.; Sponer, J. Quantum Chemical Benchmark Study on 46 RNA Backbone Families Using a Dinucleotide Unit. *J. Chem. Theory Comput.* **2015**, *11*, 4972–4991.

(86) Eshuis, H.; Furche, F. Basis set convergence of molecular correlation energy differences within the random phase approximation. *J. Chem. Phys.* **2012**, *136*, 084105.

(87) Weigend, F. A fully direct RI-HF algorithm: Implementation, optimised auxiliary basis sets, demonstration of accuracy and efficiency. *Phys. Chem. Chem. Phys.* **2002**, *4*, 4285–4291.

(88) Weigend, F.; Ahlrichs, R. Balanced basis sets of split valence, triple zeta valence and quadruple zeta valence quality for H to Rn: Design and assessment of accuracy. *Phys. Chem. Chem. Phys.* **2005**, *7*, 3297–3305.

(89) Weigend, F.; Furche, F.; Ahlrichs, R. Gaussian basis sets of quadruple zeta valence quality for atoms H-Kr. *J. Chem. Phys.* **2003**, *119*, 12753.

(90) Dunning, T. H. Gaussian basis sets for use in correlated molecular calculations. I. The atoms boron through neon and hydrogen. *J. Chem. Phys.* **1989**, *90*, 1007.

(91) Woon, D. E.; Dunning, T. H. Gaussian basis sets for use in correlated molecular calculations. III. The atoms aluminum through argon. *J. Chem. Phys.* **1993**, *98*, 1358–1371.

(92) Hättig, C. Optimization of auxiliary basis sets for RI-MP2 and RI-CC2 calculations: Core-valence and quintuple-ζ basis sets for H to Ar and QZVPP basis sets for Li to Kr. *Phys. Chem. Chem. Phys.* **2005**, *7*, 59–66.

(93) Weigend, F.; Köhn, A.; Hättig, C. Efficient use of the correlation consistent basis sets in resolution of the identity MP2 calculations. *J. Chem. Phys.* **2002**, *116*, 3175–3183.

(94) Peterson, K. A.; Figgen, D.; Goll, E.; Stoll, H.; Dolg, M. Systematically convergent basis sets with relativistic pseudopotentials. II. Small-core pseudopotentials and correlation consistent basis sets for the post-d group 16–18 elements. *J. Chem. Phys.* **2003**, *119*, 11113–11123.

(95) Peterson, K. A.; Shepler, B. C.; Figgen, D.; Stoll, H. On the Spectroscopic and Ther-

mochemical Properties of ClO, BrO, IO, and Their Anions. *J. Phys. Chem. A* **2006**, *110*, 13877–13883.

(96) Risthaus, T.; Grimme, S. Benchmarking of London Dispersion-Accounting Density Functional Theory Methods on Very Large Molecular Complexes. *J. Chem. Theory Comput.* **2013**, *9*, 1580–1591.

(97) Halkier, A.; Helgaker, T.; Jørgensen, P.; Klopper, W.; Koch, H.; Olsen, J.; Wilson, A. K. Basis–set convergence in correlated calculations on Ne, N_2, and H_2O. *Chem. Phys. Lett.* **1998**, *286*, 243–252.

(98) Luenser, A.; Schurkus, H. F.; Ochsenfeld, C. Vanishing-Overhead Linear-Scaling Random Phase Approximation by Cholesky Decomposition and an Attenuated Coulomb-Metric. *J Chem. Theory Comput.* **2017**, *13*, 1647–1655.

(99) Zhao, Y.; Truhlar, D. G. A new local density functional for main-group thermochemistry, transition metal bonding, thermochemical kinetics, and noncovalent interactions. *J. Chem. Phys.* **2006**, *125*, 194101.

(100) Sun, J.; Ruzsinszky, A.; Perdew, J. P. Strongly Constrained and Appropriately Normed Semilocal Density Functional. *Phys. Rev. Lett.* **2015**, *115*, 036402.

(101) Brandenburg, J. G.; Bates, J. E.; Sun, J.; Perdew, J. P. Benchmark tests of a strongly constrained semilocal functional with a long-range dispersion correction. *Phys. Rev. B* **2016**, *94*, 115144.

(102) Jansen, G. Symmetry-adapted perturbation theory based on density functional theory for noncovalent interactions. *Wiley Interdiscip. Rev. Comput. Mol. Sci.* **2014**, *4*, 127–144.

(103) Misquitta, A. J.; Jeziorski, B.; Szalewicz, K. Dispersion Energy from Density-Functional Theory Description of Monomers. *Phys. Rev. Lett.* **2003**, *91*, 033201.

(104) Wesolowski, T. A.; Warshel, A. Frozen density functional approach for ab initio calculations of solvated molecules. *J. Phys. Chem.* **1993**, *97*, 8050–8053.

(105) Kevorkyants, R.; Eshuis, H.; Pavanello, M. FDE-vdW: A van der Waals inclusive subsystem density-functional theory. *J. Chem. Phys.* **2014**, *141*, 044127.

(106) Hohenberg, P.; Kohn, W. Inhomogeneous Electron Gas. *Phys. Rev.* **1964**, *136*, B864–B871.

(107) Ćwiok, T.; Jeziorski, B.; Kol/os, W.; Moszynski, R.; Szalewicz, K. On the convergence of the symmetrized Rayleigh-Schrödinger perturbation theory for molecular interaction energies. *J. Chem. Phys.* **1992**, *97*, 7555–7559.

(108) Cohen, M. H.; Wasserman, A. On Hardness and Electronegativity Equalization in Chemical Reactivity Theory. *J. Stat. Phys.* **2006**, *125*, 1121–1139.

(109) Elliott, P.; Burke, K.; Cohen, M. H.; Wasserman, A. Partition density-functional theory. *Phys. Rev. A* **2010**, *82*, 024501.

(110) Görling, A.; Levy, M. Correlation-energy functional and its high-density limit obtained from a coupling-constant perturbation expansion. *Phys. Rev. B* **1993**, *47*, 13105–13113.

(111) Görling, A.; Levy, M. Hardness of molecules and the band gap of solids within the Kohn–Sham formalism: A perturbation-scaling approach. *Phys. Rev. A* **1995**, *52*, 4493–4499.

(112) Eshuis, H.; Bates, J. E.; Furche, F. Electron correlation methods based on the random phase approximation. *Theor. Chem. Acc.* **2012**, *131*, 1084.

(113) Furche, F. Developing the random phase approximation into a practical post-Kohn-Sham correlation model. *J. Chem. Phys.* **2008**, *129*, 114105.

(114) Craig, D. P.; Thirunamachandran, T. *Molecular quantum electrodynamics: an introduction to radiation-molecule interactions*; Courier Corporation, 1998.

(115) Szalewicz, K. Symmetry-adapted perturbation theory of intermolecular forces. *Wiley Interdiscip. Rev.: Comput. Mol. Sci.* **2012**, *2*, 254–272.

(116) Fetter, A. L.; Walecka, J. D. *Quantum Theory of Many-Particle Systems*; McGraw-Hill, 1971.

(117) Cappellini, G.; Del Sole, R.; Reining, L.; Bechstedt, F. Model dielectric function for semiconductors. *Phys. Rev. B* **1993**, *47*, 9892–9895.

(118) Brawand, N. P.; Vörös, M.; Govoni, M.; Galli, G. Generalization of Dielectric-Dependent Hybrid Functionals to Finite Systems. *Phys. Rev. X* **2016**, *6*, 041002.

(119) Longuet-Higgins, H. C. Spiers Memorial Lecture. Intermolecular forces. *Discuss. Faraday Soc.* **1965**, *40*, 7–18.

(120) Zaremba, E.; Kohn, W. Van der Waals interaction between an atom and a solid surface. *Phys. Rev. B* **1976**, *13*, 2270–2285.

(121) Horn, R. A.; Mathias, R. Cauchy-Schwarz inequalities associated with positive semidefinite matrices. *Linear Algebra and its Applications* **1990**, *142*, 63 – 82.

(122) Chen, G. P.; Agee, M. M.; Furche, F. Performance and Scope of Perturbative Corrections to Random-Phase Approximation Energies. *J. Chem. Theory Comput.* **2018**, *14*, 5701–5714.

(123) Kato, T. *Perturbation theory for linear operators*; Springer Science & Business Media, 2013; Vol. 132.

(124) Olsen, J.; Jørgensen, P.; Helgaker, T.; Christiansen, O. Divergence in Møller–Plesset theory: A simple explanation based on a two-state model. *J. Chem. Phys.* **2000**, *112*, 9736–9748.

(125) Gould, T.; Toulouse, J.; Ángyán, J. G.; Dobson, J. F. Casimir-Polder Size Consistency: A Constraint Violated by Some Dispersion Theories. *J. Chem. Theory Comput.* **2017**, *13*, 5829–5833.

(126) Scuseria, G. E.; Henderson, T. M.; Sorensen, D. C. The ground state correlation energy of the random phase approximation from a ring coupled cluster doubles approach. *J. Chem. Phys.* **2008**, *129*, 231101.

(127) Toulouse, J.; Zhu, W.; Savin, A.; Jansen, G.; Ángyán, J. G. Closed-shell ring coupled cluster doubles theory with range separation applied on weak intermolecular interactions. *J. Chem. Phys.* **2011**, *135*, 084119.

(128) Dzyaloshinskii, I.; Lifshitz, E.; Pitaevskii, L. The general theory of van der Waals forces. *Adv. Phys.* **1961**, *10*, 165–209, cited By 1257.

(129) Bohm, D.; Pines, D. A Collective Description of Electron Interactions. I. Magnetic Interactions. *Phys. Rev.* **1951**, *82*, 625–634.

(130) Pines, D.; Bohm, D. A Collective Description of Electron Interactions: II. Collective vs Individual Particle Aspects of the Interactions. *Phys. Rev.* **1952**, *85*, 338–353.

(131) Yan, Z.; Perdew, J. P.; Kurth, S. Density functional for short-range correlation: Accuracy of the random-phase approximation for isoelectronic energy changes. *Phys. Rev. B* **2000**, *61*, 16430–16439.

(132) Yan, Z.; Perdew, J. P.; Kurth, S. Erratum: Density functional for short-range correlation: Accuracy of the random-phase approximation for isoelectronic energy changes [Phys. Rev. B 61, 16430 (2000)]. *Phys. Rev. B* **2010**, *81*, 169902.

(133) Ajala, A. O.; Voora, V.; Mardirossian, N.; Furche, F.; Paesani, F. Assessment of Density Functional Theory in Predicting Interaction Energies between Water and

Polycyclic Aromatic Hydrocarbons: from Water on Benzene to Water on Graphene. *J. Chem. Theory and Comput.* **2019**, *15*, 2359–2374.

(134) Shepherd, J. J.; Grüneis, A. Many-Body Quantum Chemistry for the Electron Gas: Convergent Perturbative Theories. *Phys. Rev. Lett.* **2013**, *110*, 226401.

(135) Grüneis, A.; Marsman, M.; Harl, J.; Schimka, L.; Kresse, G. Making the random phase approximation to electronic correlation accurate. *J. Chem. Phys.* **2009**, *131*, 154115.

(136) Paier, J.; Janesko, B. G.; Henderson, T. M.; Scuseria, G. E.; Grüneis, A.; Kresse, G. Hybrid functionals including random phase approximation correlation and second-order screened exchange. *J. Chem. Phys.* **2010**, *132*, 094103.

(137) Paier, J.; Janesko, B. G.; Henderson, T. M.; Scuseria, G. E.; Grüneis, A.; Kresse, G. Erratum: "Hybrid functionals including random phase approximation correlation and second-order screened exchange" [J. Chem. Phys. 132, 094103 (2010)]. *J. Chem. Phys.* **2010**, *133*, 179902.

(138) Bates, J. E.; Furche, F. Communication: Random phase approximation renormalized many-body perturbation theory. *J. Chem. Phys.* **2013**, *139*, 171103.

(139) Jones, A. P.; Crain, J.; Sokhan, V. P.; Whitfield, T. W.; Martyna, G. J. Quantum Drude oscillator model of atoms and molecules: Many-body polarization and dispersion interactions for atomistic simulation. *Phys. Rev. B* **2013**, *87*, 144103.

(140) Hermann, J.; DiStasio, R. A.; Tkatchenko, A. First-Principles Models for van der Waals Interactions in Molecules and Materials: Concepts, Theory, and Applications. *Chem. Rev.* **2017**, *117*, 4714–4758.

(141) Heßelmann, A. Random-phase-approximation correlation method including exchange interactions. *Phys. Rev. A* **2012**, *85*, 012517.

(142) Riplinger, C.; Neese, F. An efficient and near linear scaling pair natural orbital based local coupled cluster method. *J. Chem. Phys.* **2013**, *138*, 034106.

(143) Kallay, M. Linear-scaling implementation of the direct random-phase approximation. *J. Chem. Phys.* **2015**, *142*, 204105.

(144) Chen, G. P.; Voora, V. K.; Agee, M. M.; Balasubramani, S. G.; Furche, F. Random-Phase Approximation Methods. *Annu. Rev. Phys. Chem.* **2017**, *68*, 421–445.

(145) Schurkus, H. F.; Ochsenfeld, C. Communication: An effective linear-scaling atomic-orbital reformulation of the random-phase approximation using a contracted double-Laplace transformation. *J. Chem. Phys.* **2016**, *144*, 031101.

(146) Beuerle, M.; Ochsenfeld, C. Low-scaling analytical gradients for the direct random phase approximation using an atomic orbital formalism. *J. Chem. Phys.* **2018**, *149*, 244111.

(147) Graf, D.; Beuerle, M.; Ochsenfeld, C. Low-Scaling Self-Consistent Minimization of a Density Matrix Based Random Phase Approximation Method in the Atomic Orbital Space. *J. Chem. Theory Comput.* **2019**, *15*, 4468–4477.

(148) Voora, V. K.; Balasubramani, S. G.; Furche, F. Variational generalized Kohn-Sham approach combining the random-phase-approximation and Green's-function methods. *Phys. Rev. A* **2019**, *99*, 012518.

(149) Muuronen, M.; Deglmann, P.; Tomović, Ž. Design Principles for Rational Polyurethane Catalyst Development. *J. Org.* **2019**, *84*, 8202–8209.

Graphical TOC Entry